Master Thesis

Studies of Solar Magnetic Cancellation: Dynamics and its Association with the Filament Formation

Yusuke Iida

Department of Earth and Planetary Science
Graduate School of Science, The University of Tokyo

February, 26, 2009

Abstract

A cancellation is defined as a disappearance of positive and negative vertical magnetic patches on the solar photosphere. A cancellation is a basic process of photospheric magnetic field and plays an important role in the photospheric magnetic flux balance. It also has important roles in the various solar activities, e.g. XBPs (X-ray bright points), solar filament formations, flares. Photospheric cancellations has been observed since 1980s and two theoretical scenarios are suggested, the "U-loop emergence" scenario and the "Ω-loop submergence" scenario. However, because it needs stable high temporal and spatial resolution, the theoretical scenarios have not been distinguished by observations yet. It is very important to distinguish these theoretical scenarios for comprehension of the solar magnetic field dynamics and the solar activity structures. Our purpose of the former part of this thesis is a distinction of cancellation scenarios by an observation. The latter part is devoted to a determination of solar filament formation models.

"*Hinode*" satellite, launched in September 2006, achieves the stable high temporal and spatial resolution. In chapter 2 of this thesis, we determine the three components of magnetic field and velocity structure of the cancellations in the quiet Sun using "*Hinode*". We found the horizontal magnetic field connecting the canceling magnetic features (CMFs) and the characteristic downflow around the cancellation sites. We interpreted the observed cancellations as the "Ω-loop submergence" from these results.

In chapter 3 of this thesis, we determine the association of solar filament formations, photspheric cancellations, and brightenings in the Extreme Ultra Violet (EUV) images. The filament formation models can be mainly divided into two categories. One is the flux emergence model and the other is the reconnection model. These models are based on the fact that a photospheric cancellation is a necessary condition for a filament formation. We statistically determined the simultaneous events of a filament formation and photospheric cancellations. We used the full-disk Hα images taken by Hida/SMART (Kyoto University), the full-disk LOS magnetic field images by SOHO/MDI. We found filament formations without photospheric cancellations. The simple flux emergence model can not explain this result. We interpret the EUV brightenings as the signature of magnetic reconnection. In the quiet Sun, the ratio of the EUV brightening is large. We also observed the filament formations after EUV brightenings in some events. We conclude that the reconnection model is dominant in the quiet Sun.

要旨

太陽光球の視線方向磁場の正極と負極が衝突し、それらの一部もしくはすべてが消滅する現象を光球磁場キャンセレーションという。キャンセレーションは光球磁場の基礎的な活動であり、その収支に大きな役割を果たしていると考えられている。また、X 線輝点・太陽フィラメント形成・フレアなどの様々な太陽面活動と密接に関係があるとされている。光球磁場キャンセレーションは 1980 年代から観測されている。また、その理論的モデルとして U 字型ループ上昇・Ω 字型ループ沈降が提案されている。しかしながら、詳細な構造の観測には安定した高時間・空間分解能が要求されることから、未だに理論モデルが観測で区別されたとは言えない。これらの物理モデルの区別は、太陽における磁場の運動、太陽表面活動における磁場構造の把握につながるため非常に重要である。本論文の前半部では観測から物理モデルの区別を行うこと、後半部では太陽フィラメントの形成とキャンセレーションの関係を調べモデルについて区別することを目標とした。

2006 年 9 月に打ち上げられた「ひので」衛星はいままでにない安定した高時間・空間分解能を実現している。本研究の前半部では、「ひので」衛星からのデータを用いて、静穏領域における光球磁場キャンセレーションの 3 成分磁場・速度場構造を調べた。その結果、キャンセレーションが起こるときにそれぞれの磁極を結ぶ向きの水平磁場が確認された。また、キャンセレーション領域において特徴的な下降流が見られた。これらの特徴から、対象のキャンセレーション領域においては Ω 字型沈降が起こっていると結論づけた。

本研究の後半部では、太陽フィラメントの形成・光球磁場キャンセレーション・極紫外線 (EUV) での増光現象の関係を調べた。太陽フィラメントの形成には大きく分けて磁束管浮上モデルと磁気リコネクションモデルがある。これらのモデルはフィラメント形成には光球磁場キャンセレーションが必要条件であるという観測事実に基づいて考えられている。そこで本研究では京都大学飛騨天文台の SMART による太陽全面 Hα 線画像、SOHO/MDI による太陽全面視線方向磁場画像を用いて、フィラメント形成に対して光球磁場キャンセレーションの発生の有無を統計的に調べた。その結果、光球磁場キャンセレーションの見られないフィラメント形成が多く見られた。これは単純な磁気浮上モデルでは説明できないことである。さらに、リコネクションが起きているかを確認するためにフィラメント形成と EUV 増光の関係を調べた。その結果、静穏領域のキャンセレーションが見られないフィラメント形成において、EUV 増光が見られる割合が多いことが分かった。また、いくつかのイベントでは EUV 増光の後にフィラメント形成をみることができた。これらの結果から、静穏領域のフィラメント形成では磁気リコネクションモデルが支配的であると結論した。

Contents

Abstract **2**

Table of Contents **6**

List of Figures **8**

List of Tables **9**

1 General Introduction **10**

2 The Vector Magnetic Fields and Velocity Structures at the Cancellation Sites **15**
2.1 Introduction . . . 15
2.2 *Hinode* Satellite . . . 17
2.2.1 SOT/FG . . . 17
2.2.2 SOT/SP . . . 18
2.3 Data selection and Analysis . . . 19
2.3.1 Magnetic Fields . . . 21
2.3.2 Velocity Fields . . . 22
2.4 Results . . . 22
2.4.1 Time Series of a Typical Cancellation . . . 23
2.4.2 Horizontal Magnetic Fields between canceling magnetic patches . . . 23
2.4.3 Velocity Fields around the Cancellation Sites . . . 26
2.4.4 Time Series of the Magnetic Flux and Velocity Structures . . . 27
2.5 Discussions . . . 27
2.5.1 Horizontal Magnetic Fields Connecting the CMFs . . . 27
2.5.2 Dominant Downflow around the Cancellation Sites . . . 29
2.5.3 An Estimation of the Submerged Magnetic Flux . . . 30
2.5.4 What is the "Ω-loop submergence" mechanism? . . . 30
2.6 Summary and Future Works . . . 30

3 Association between the Cancellations and the Filament Formations **33**
3.1 Introduction . . . 33
3.2 Instrumentation . . . 35
3.3 Analysis . . . 36

3.3.1 Event Selection 36
3.3.2 Detection criteria of Filament Formations 37
3.3.3 Detection criteria of Cancellations 37
3.3.4 Detection criteria of EUV Brightenings 38
3.3.5 Comparison of Filament Formations, Cancellations, and EUV Brightenings 38
3.4 Results 38
3.4.1 Filament Formations and Simultaneous Cancellations 38
3.4.2 Filament Formations and Simultaneous EUV Brightenings 39
3.4.3 Statistical Results 41
3.5 Discussions 42
3.5.1 Filament Formations and Cancellations 43
3.5.2 Filament Formations and EUV Brightenings 43
3.5.3 Filament Formation Models 44
3.6 Summary and Future Works 44

Acknowledgment **45**

List of Figures

1.1 Solar magnetic field and corona activities: (Left) The line-of-sight magnetic field image by SOHO/MDI (Right) X-ray image by *Hinode*/XRT. 11
1.2 The line-of-sight magnetic flux density observed by MDI is displayed. White (black) color corresponds to the positive (negative) polarity. 11
1.3 Schematic pictures of "U-loop emergence" and "Ω-loop submergence" for a magnetic cancellation. 12
1.4 Dark filaments and solar prominences in an Hα image taken by Big Bear Solar Observatory (BBSO). 13

2.1 A timing differrence of a photospheric cancellation and a chromospheric cancellation from Harvey et al (1999) 16
2.2 A LOS magnetic field, transversal magnetic field, and Doppler velocity map around a cancellation site from Chae et al. (2004) 16
2.3 The center-to-limb variation of the doppler velocity around the cancellation sites from Kubo et al. (2007) 17
2.4 The appearance of the "*Hinode*" satellite (http://hinode.nao.ac.jp). 18
2.5 The data taken by SOT/SP in the fast mode. Each panel from left shows the Stokes-I, Q, U and V, respectively. The horizontal axis is the wavelength from 6300.8Å to 6303.2Å. The vertical axis is the solar y-coordinate in unit of 0.32 arcsec. Note the dark vertical features found in Stokes I are the Fe I lines at 6301.5 Å and 6302.5 Å. 19
2.6 The spectrogram taken by SOT/SP. The horizontal axis is the wavelength. Unit of intensity is DN. 20
2.7 A schematic picture of Stokes-V profile. $V-b$ (V_r) is the blue (red) side of the observational wavelength. As the LOS magnetic field becomes stronger, the amplitude of V-signal arises and $G = V_b - V_r$ becomes bigger. 21
2.8 A schematic picture of Stokes-I profile with Doppler shift. Blue line, black line, and red line mean blue shift, no Doppler shift, and red shift respectively. $F = \frac{I_b - I_r}{I_b + I_r}$ becomes negative in blue shift, zero in no Doppler shift, and positive in red shift. 22
2.9 Theoretical relationship between the Doppler velocity and F. We calculate from the Atlas profile and the trancemittance spectrum of the filtergram. Doppler velocity and F are proportional. 23

2.10 Time series of G signal (see Eq.2.1) in NaI 5869Å from SOT/FG on 2007 October 31th. The field of view is 20 arcsec × 20 arcsec. 24
2.11 Magnetic fields obtained by the Milne-Eddington fitting of the Hinode/SP data on 2007 October 31. The maximum magnetic strength is ∼300G. The LOS component is shown in contours. Yellow (Blue) lines are for positive (negative) polarities for 100 and 300G. (Top) Magnetic strength of transversal component in gray scale map. (Bottom) Transversal component is shown by arrows. The longest arrow corresponds 300G. The transversal field between the magnetic patches is aligned as connecting each other. 25
2.12 The Doppler velocity field obtained by using NaI Stokes-I from SOT/FG. The background is LOS velocity and the contour is LOS magnetic field. The red (blue) background indicates the downflow (upflow) and white (black) contour indicates positive (negative) vertical field. The field of view is 10 arcsec × 10 arcsec. The plotted range of LOS velocity is from −2.0 km/s to 2.0 km/s. . . 26
2.13 The Doppler velocity field summed over 5 minutes from SOT/FG. The background is LOS velocity and the contour is LOS magnetic field. The field of view and colors are same as Fig.2.12. The plotted range of LOS velocity is from −2.0 km/s to 2.0 km/s. 27
2.14 The time evolution of magnetic flux of the cancellation. We integrate Stokes-V around the cancellation site. The solid (dotted) line is positive (negative) flux. The cancellation occurs between 16:42 to 17:20. 28
2.15 A schematic picture of Ω-loop submergence. The downflow can be seen at the footpoint of Ω-loop at first and in the same position with the horizontal field later. 29
2.16 Schematic pictures of a cancellation scenario. Two magnetic flux rope are convected by the supergranultaion. When they get close, a magnetic reconnection happens in the solar chromosphere or corona. They continue to converge after the reconnection. The newly formed magnetic fields submerge by magnetic tension when they get closer than a few times of scale height. 31

3.1 The flux emergence model from Zwaan (1987). We can see the vertical magnetic patches converge at the photosphere when the magnetic flux emerges from below the photosphere. 34
3.2 The Head-to-linkage model from Martens & Zwaan (2001). The dotted line is the polarity inversion line at the photosphere. There are photospheric cancellations when the magnetic reconnection occurs. 35
3.3 An example of filament formations. We can see the filament formation more than 50 arcsec. These images are from SMART/Hida Observatory. 37
3.4 A simultaneous event of filament formation and a photospheric cancellation. . 39
3.5 A filament formation without photospheric cancellations. The arrows indicate the formation point. 40
3.6 EUV images of a filament formation without cancellations. The arrows indicate the EUV brightening. We can see a filament formation in EUV images. . 41

List of Tables

3.1 The ratio of filament formations with cancellations. 42
3.2 The ratio of EUV brightenings to filament formations. 42

Chapter 1

General Introduction

We can see that the solar surface is filled with the magnetic field when observing by polarization measurement in the visible light. There are magnetic fields in active regions and even in quiet regions. These magnetic fields are thought to play some important roles in the various solar activities, e.g. X-ray bright points (XBPs), filament formations, solar flares and solar dynamo (see Fig.1.1). The magnetic fields of the solar surface has been observed since long time ago. However, we have not understood the dynamics of the magnetic field itself and its association with the solar activities very much.

When we observe the magnetic field in the photosphere, we can notice that the magnetic fields are moving as the magnetic patches. The phenomena of the magnetic patches has a wide variety (Livi et al., 1985; Martin et al., 1985). Some patches are emerging, splitting or disappearing. These magnetic activities are reported in 1980s. A photospheric cancellation is one of the basic magnetic activities (see Fig.1.2). A convergence and disappearance of positive and negative magnetic patches are defined as a cancellation (Martin et al, 1985). A cancellation contributes to the decrease of the photospheric magnetic field directly and is believed to be a main activity for photospheric magnetic flux removal. It can be said that it is important for the comprehension of the photospheric magnetic balance to interpret cancellations correctly.

Cancellations can be interpreted as the flux transports between the solar interior and the solar atmosphere. Fig.1.3 shows schematic pictures of a cancellation (Zwaan, 1987). The left image shows the "U-loop emergence". The Line-of-sight (LOS) magnetic patches are the emerging points of U-loop. As the magnetic loop ascends, the patches converge. Finally the magnetic patches disappear when the U-loop rises to the solar atmosphere totally. A cancellation is observed as a result of a flux rope emergence from below the photosphere to the solar atmosphere. In this model, the magnetic flux on the photosphere decreases and the magnetic field is transported from below the photosphere to the solar atmosphere. The right panel shows the "Ω-loop submergence". The magnetic patches are the foot-points of the submerging Ω-loop in the solar atmosphere. As the Ω loop submerges, the magnetic patches are converging toward each other. When the Ω-loop submerges totally, the converging magnetic patches disappear. In this scenario, the magnetic flux on the photosphere decreases and the magnetic field is transported from the solar atmosphere to below the photosphere. These

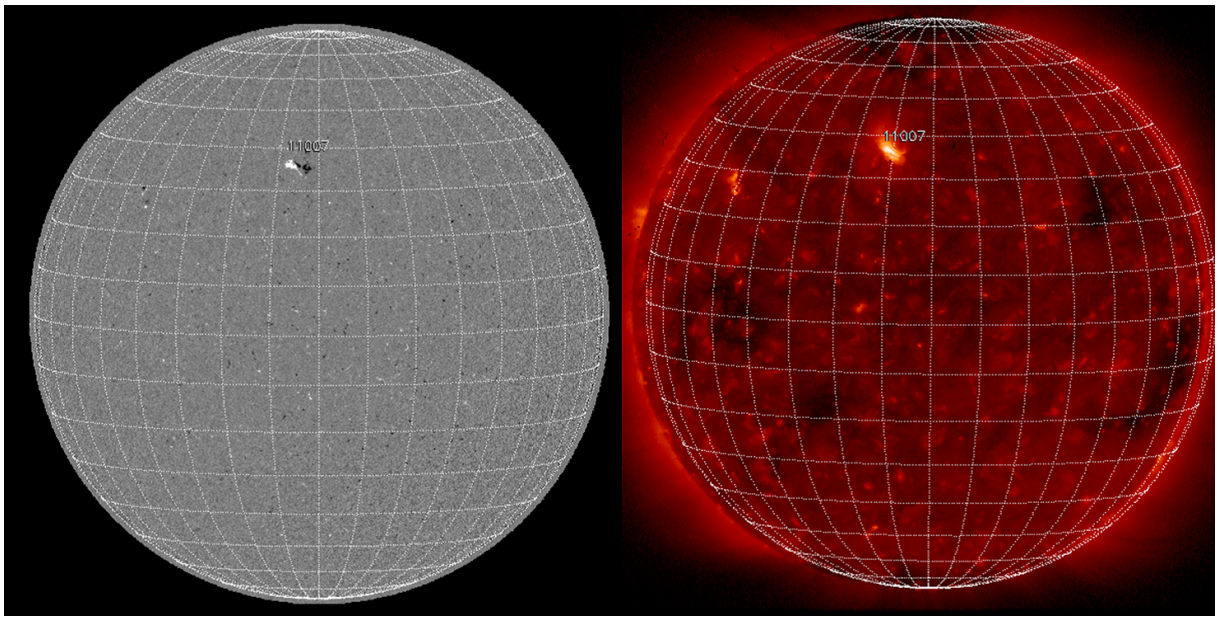

Figure 1.1: Solar magnetic field and corona activities: (Left) The line-of-sight magnetic field image by SOHO/MDI (Right) X-ray image by *Hinode*/XRT.

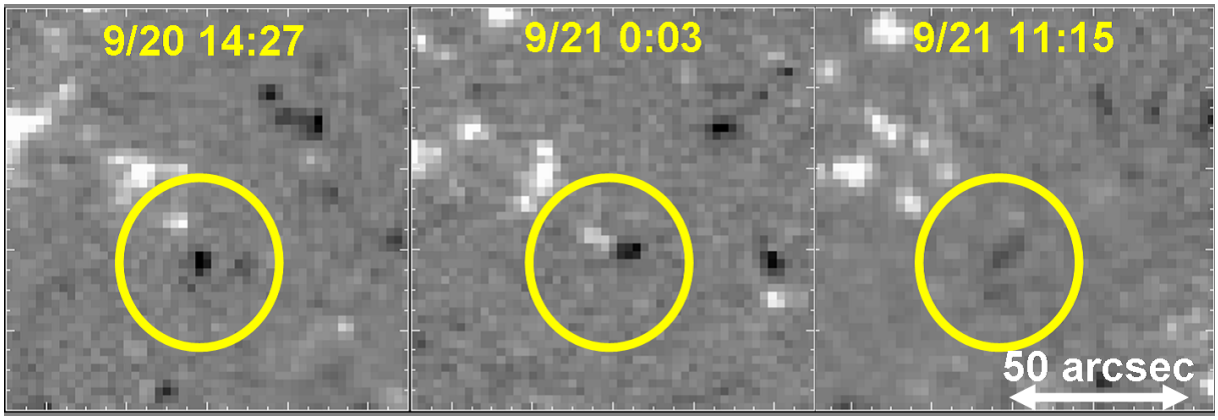

Figure 1.2: The line-of-sight magnetic flux density observed by MDI is displayed. White (black) color corresponds to the positive (negative) polarity.

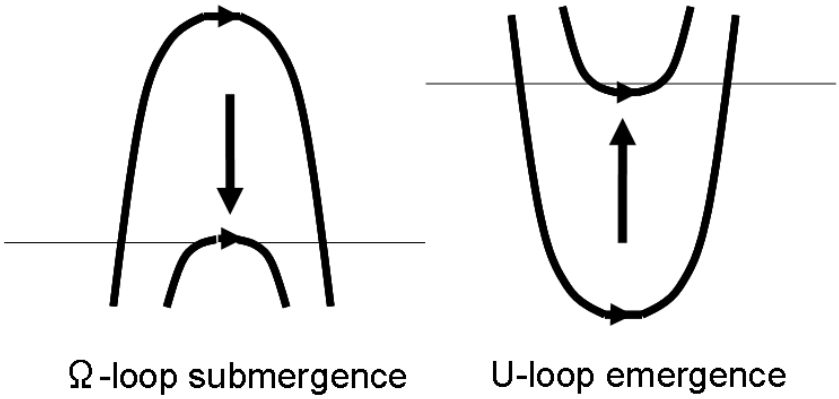

Figure 1.3: Schematic pictures of "U-loop emergence" and "Ω-loop submergence" for a magnetic cancellation.

two scenarios are same in the photospheric magnetic flux balance but opposite in the flux transport between the solar interior and the atmosphere. From a theoretical speculation, the U-loop emergence scenario seems to be preferable because the magnetic buoyancy force may drive magnetic flux emerging rather than submerging. But which of these theoretical models is dominant in the actual cancellations?

From an observational point of view, there are some papers which reports the magnetic and velocity field at the cancellation sites. Harvey et al. tried this problem by comparing a timing difference of photospheric and chromospheric cancellations (Harvey et al., 1999). They obtained the result that the "Ω-loop submergence" is dominant (44%) in quiet regions. But this is an indirect evidence of "Ω-loop submergence". In response to this result, Chae et al. investigated the magnetic and Doppler velocity field at the cancellations by a spectro-polarization measurement (Chae et al., 2004). They found the strong horizontal magnetic field and the downflow at the cancellation sites. This is the first direct observation of horizontal field and velocity structures at the cancellation sites. The downflow velocity is ~1km/s. But the temporal resolution was not good (~26minutes) enough to pursue the time evolution of these structures and only two active region cancellations are investigated.

Though a cancellation is an important clue for both the photospheric flux balance and the flux transportation between the solar interior and the solar atmosphere, the magnetic and velocity structures of a cancellation are not understood well. The direct observation of the velocity fields in the previous studies are all about active region cancellations. There are no reports on the quiet Sun cancellations. In chapter 2 of this thesis, we investigate the vector magnetic field and velocity structures around the cancellation sites.

A cancellation is also said to have some important roles in various solar activities. Solar filament formation is one example. A solar filament and a solar prominence are the same activities. When it is observed at the limb, it is called solar prominence and when observed on the solar disk, it is called a dark filament (see Fig.1.4). Filaments are very impressive solar activities known from long time ago not only because we can observe them in visible

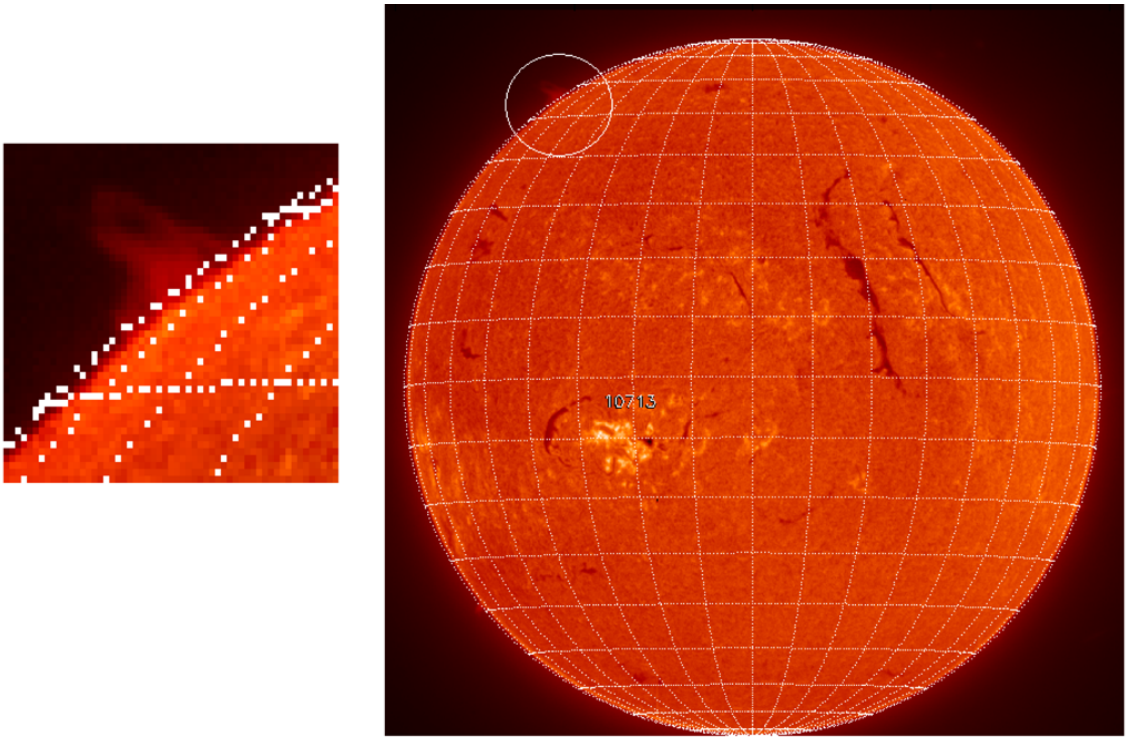

Figure 1.4: Dark filaments and solar prominences in an Hα image taken by Big Bear Solar Observatory (BBSO).

light but also they suddenly erupt and sometimes affect the Earth as Coronal Mass Ejections (CME).

Filaments attract many scientists but their physical structures and their lives are still not known. One of the main mystery about the filaments is their formation process. Though we sometimes see filaments longer than 500 arcsec, which is half of the solar radius, the formation mechanism is not known yet. We already know the magnetic field in the photosphere has an important role in the filament formations, because filaments are always on the polarity inversion line (PIL) and a cancellation is a necessary condition for filament formations (Bobcock & Bobcock, 1954; Howard, 1985; Livi et al., 1985; Martin et al., 1985). Based on these conditions, a lot of models are suggested. These models can be divided into two categories. One is the flux emergence models and the other is the reconnection models (Kippenhahn & Schlüter, 1957; Kuperus & Raadu, 1974; van Ballegooijen & Martens, 1989; Martens & Zwaan, 2001). These models are difficult to separate only by the observations of photospheric magnetic field but could be discriminated by a investigation of additional simultaneous observations of Hα images and extreme ultra violet (EUV) images.

We investigate the association among a filament formation, a photospheric cancellation, and an EUV brightening in chapter 3 of this thesis. Our purpose of that chapter is to discuss the validation of these two filament formation models.

The main part of this thesis is Chapter 2 and Chapter 3. We investigate the vector magnetic field and velocity structures around the cancellation site in the quiet Sun in Chapter 2. Our purpose in Chapter 2 is to investigate the cancellations in quiet Sun. In Chapter.3, we investigate the relationship among filament formations, photospheric cancellations, and EUV brightenings.

Chapter 2

The Vector Magnetic Fields and Velocity Structures at the Cancellation Sites

2.1 Introduction

The magnetic cancellation is an apparent convergence and following disappearance of positive and negative magnetic patches observed in the line-of-sight (LOS) magnetic field images of the solar photosphere. Cancellation is thought to be important not only for the photospheric magnetic flux balance but also for the various solar activities. The physical structure and the dynamics of this phenomena is, however, still not understood yet. Two theoretical scenarios are proposed. One is the "U-loop emergence" and the other is "Ω-loop submergence" (see Fig. 1.3). These two scenarios are totally different in the flux transport between below the photosphere and the solar atmosphere. "U-loop emergence" and "Ω-loop submergence" are thought to be separable by an observation of the velocity field. But from recent studies, it has become clear that it needs higher temporal and spatial resolution than we thought.

The first pioneer who investigates whether the cancellation is an emergence or submergence of flux rope is Harvey. She and her colleagues investigated whether the magnetic loop submerges or emerges from the timing difference of photospheric and chromospheric cancellations. If the cancellation occurs at the chromosphere after at the photosphere, it is thought to be a emergence and vise versa. Fig.2.1 is an example of cancellations which is thought to be a submergence where the photospheric signature preceded the chromospheric one.. Her result is that a flux submergence is the most frequent (44%) event in cancellation sites (Harvey et al., 1999). This is the first evidence of the submerging magnetic loop and a statistical analysis in quiet regions. However, it is an indirect evidence and the time resolution (~15min) is not sufficient for the detection of the timing difference between a photospheric and a chromospheric cancellation. She derives the submergence velocity by dividing the relative height between the two observed layers by the timing difference and it is about 1km/s.

After their work, Chae et al. succeeded in the direct observation of the velocity structure around the cancellation sites by using the spectroscopic analysis (Chae et al, 2004). They found the strong horizontal field and downflow (~1.0km/s) around the two cancellation sites in an active region. Fig.2.2 shows theeir results. The left panel is the vertical magnetic field.

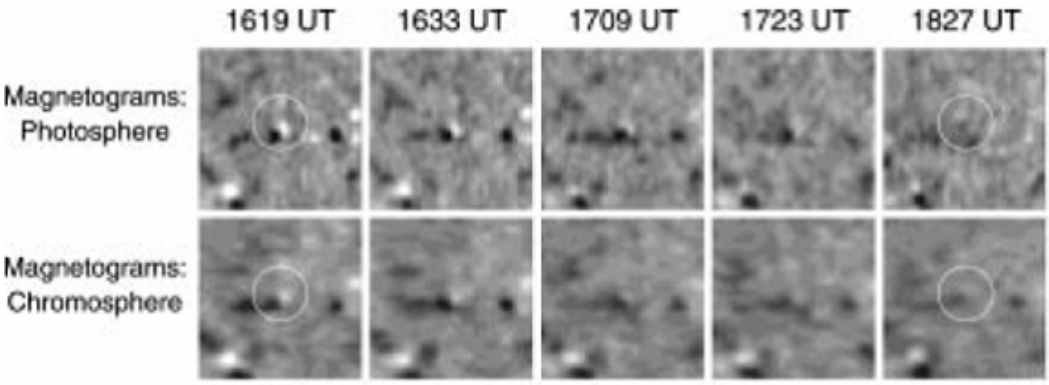

Figure 2.1: A timing differrence of a photospheric cancellation and a chromospheric cancellation from Harvey et al (1999)

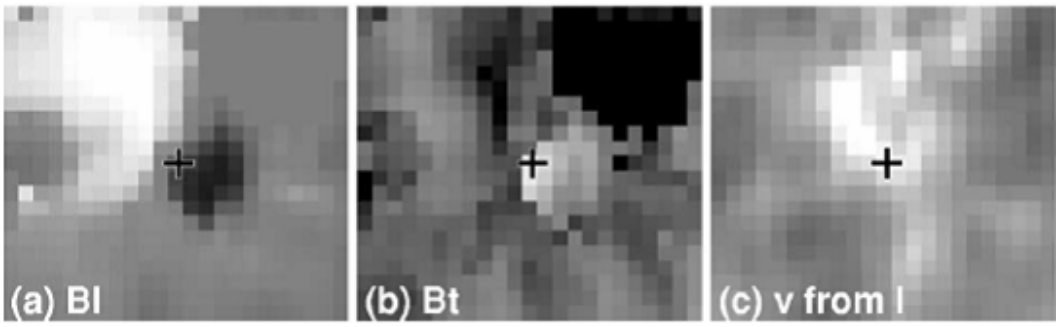

Figure 2.2: A LOS magnetic field, transversal magnetic field, and Doppler velocity map around a cancellation site from Chae et al. (2004)

We can see the canceling magnetic patches. The middle panel shows the horizontal field. We can see the horizontal magnetic field is strong between the canceling magnetic patches. The last panel is the doppler velocity obtained from the spectroscopic measurements. White background indicates the downflow and black one indicates the upflow. We can see the downflow around the cancellation. These signatures support "Ω-loop submergence" scenario. This is the first direct observation of velocity fields around a cancellation site. Time series of velocity structure is not pursued, however, because the temporal resolution is not sufficient (~26min).

Recently, Kubo et al. investigated the vector magnetic field and velocity field around the 14 cancellations in active regions (Kubo et al., 2007). The result is that there are both upflow and downflow around the cancellation sites. They also found a center-to-limb variation that the maximum value of the doppler velocity becomes larger in the limb than in the disk-center (see Fig.2.3). He concluded that these velocity structures indicate the material flow along the horizontal field.

If a pair of magnetic patches is removed from the photosphere, the flux tube must move

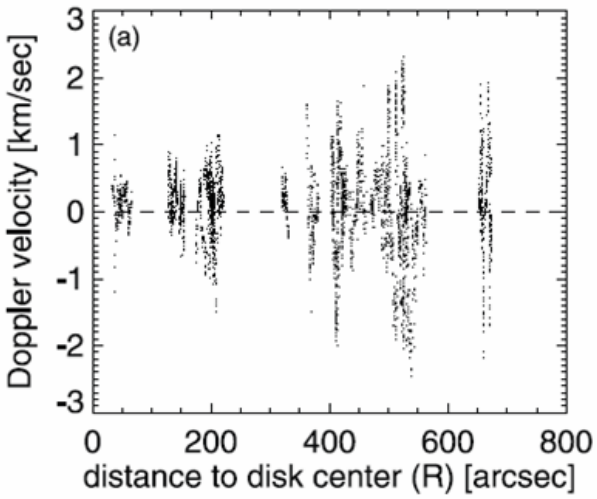

Figure 2.3: The center-to-limb variation of the doppler velocity around the cancellation sites from Kubo et al. (2007)

up-ward or down-ward. But there has not been a conclusion whether a flux tube moves up-ward or down-ward at the cancellation sites. In this chapter, we study the vector magnetic field and velocity structures of cancellations in the quiet Sun. The purpose of this study is to distinguish whether a cancellation is "U-loop emergence" or "Ω-loop submergence". The contents of this chapter is as follows. The instrument is explained in section 2. We show the analysis method in section 3 and the results in section 4. We discuss the interpretation of the observed cancellations in section 5. The conclusions and future works are in section 6.

2.2 *Hinode* Satellite

We use the data taken by *Hinode* satellite launched in September, 2006 (see Fig.2.4). "*Hinode*" has three telescopes (Kosugi et al., 2007), the Solar Optical Telescope (SOT; Tsuneta et al., 2008, Ichimoto et al., 2008, Suematsu eta l., 2008, Shimizu et al., 2008), the EUV Imaging Spectrometer (EIS), the X-Ray Telescope (XRT). These three telescopes take stable data owing to the stable observational environments in the space without the atmospheric modulations. We use SOT to investigate photospheric cancellations. The aperture of SOT is 50cm. SOT observes the various photospheric lines. SOT has two observational equipments, Filtergram (FG) and Spectro Polarimeter (SP). We make brief explanations about FG and SP in this section.

2.2.1 SOT/FG

SOT/FG is a high spatial and temporal resolution filtergram. It counts photons through the band-pass filter and FG has two band-pass filters. One is Narrowband Filter Imager (NFI)

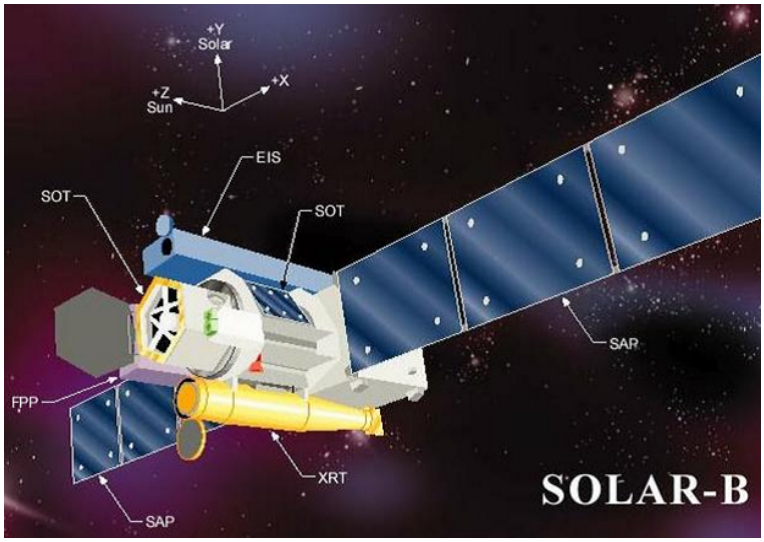

Figure 2.4: The appearance of the "*Hinode*" satellite (http://hinode.nao.ac.jp).

and the other is Broadband Filter Imager (BFI).

BFI can take filtergram images of various optical lines in high temporal and spatial resolution through the interference filter. The spatial resolution of BFI is 0.054 arcsec and maximum temporal resolution is ∼20sec. The band width of BFI is 10Å. The maximum field of view is 218 arcsec × 109 arcsec.

NFI can take filergram images in high temporal and spatial resolution through the Lyot filter. The spatial resolution of NFI is 0.08 arcsec and maximum field of view is 328 arcsec ×164 arcsec. NFI can take dopplergrams and magnetograms by polarization measurement and scanning in wave length direction. The resolution in wavelength is 0.1Å. The polarization measurement means Stokes signals, namely Stokes-I, Q, U, and V. Stokes-I is an intensity of the light. It is same as the usual filtergram data. Stokes-Q and U is linear polarization of the line. These correspond to transversal magnetic field against the LOS. Stokes-V is a circular polarization. This corresponds to the LOS magnetic fields. We have to observe at more than two wave-length if we want to observe Doppler velocity. We select two-wavelength NFI data to derive magnetic field and velocity field to take relative advantages on the time resolution rather than the spectral accuracy. If the vertical magnetogarm is needed, we have to observe Stokes-V data in addition to Stokes-I. We can choose the various lines in NFI. In this thesis, we choose NaI 5869Å line. This line is emitted from the bottom of the chromosphere. Our criteria of FG/NFI is two wave-length Stokes-I and V data of NaI 5869Å line.

2.2.2 SOT/SP

SOT/SP observes spectra around the two FeI lines, at 6301.5Å and 6302.5Å. These FeI absorption lines are formed approximately at the level in the photosphere. SP observes the four Stokes components, namely Stokes-I, Q, U, and V. Fig.2.5 shows a data taken by SOT/SP by a

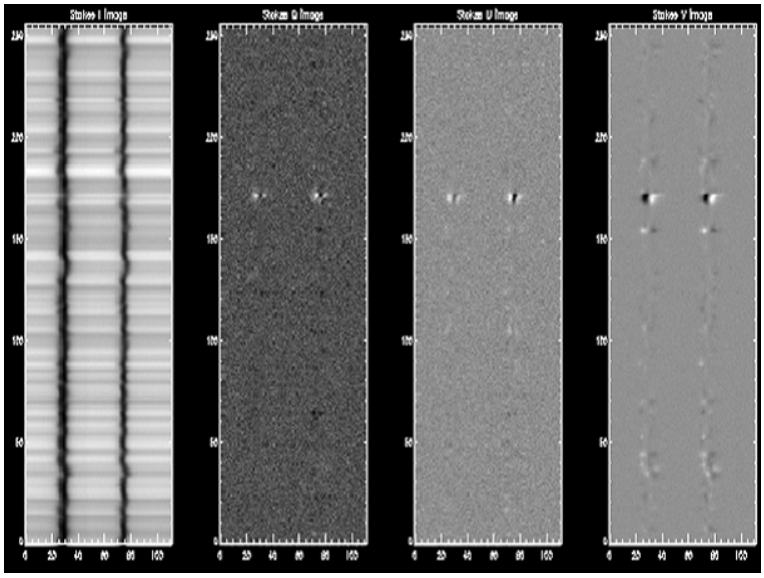

Figure 2.5: The data taken by SOT/SP in the fast mode. Each panel from left shows the Stokes-I, Q, U and V, respectively. The horizontal axis is the wavelength from 6300.8Å to 6303.2Å. The vertical axis is the solar y-coordinate in unit of 0.32 arcsec. Note the dark vertical features found in Stokes I are the Fe I lines at 6301.5 Å and 6302.5 Å.

single slit measurement. The horizontal axes of each Stokes vector are the wavelength directions and the vertical axes are spatial directions. There are two absorption lines in Stokes-I. These lines are FeI 6301.5Å and 6302.5Å. Fig.2.6 is a Stokes profile subtracted from Fig.2.5. We can see some signals in Stokes profiles of Fig.2.6. SP scans along the other spatial direction to obtain the data in two spatial dimensions, i.e. in x and y solar coordinate.. Full field of view is 168 arcsec $\times$ 328 arcsec. The number of observational points is 112 in wavelength and the resolution in wavelength is 0.03Å.

SP has three observational mode, the fast mode, normal mode, and deep mode. We can take spectra faster in fast mode than in normal mode and deep mode, but with less accuracy. If we observe full field SP data, it takes more than 60 minutes even in fast mode. In this thesis, we use fast mode data because the observation of cancellations needs high temporal resolution.

2.3 Data selection and Analysis

Our demands of data set are two wave-length FG/NFI NaI and good time resolution of SOT/SP (~30min). We select the September 10th and October 31th in 2007 on these criteria. We investigate the magnetic field and velocity structures from SOT/FG and SOT/SP. The analysis ways to derive the magnetic field and velocity field are explained in this section.

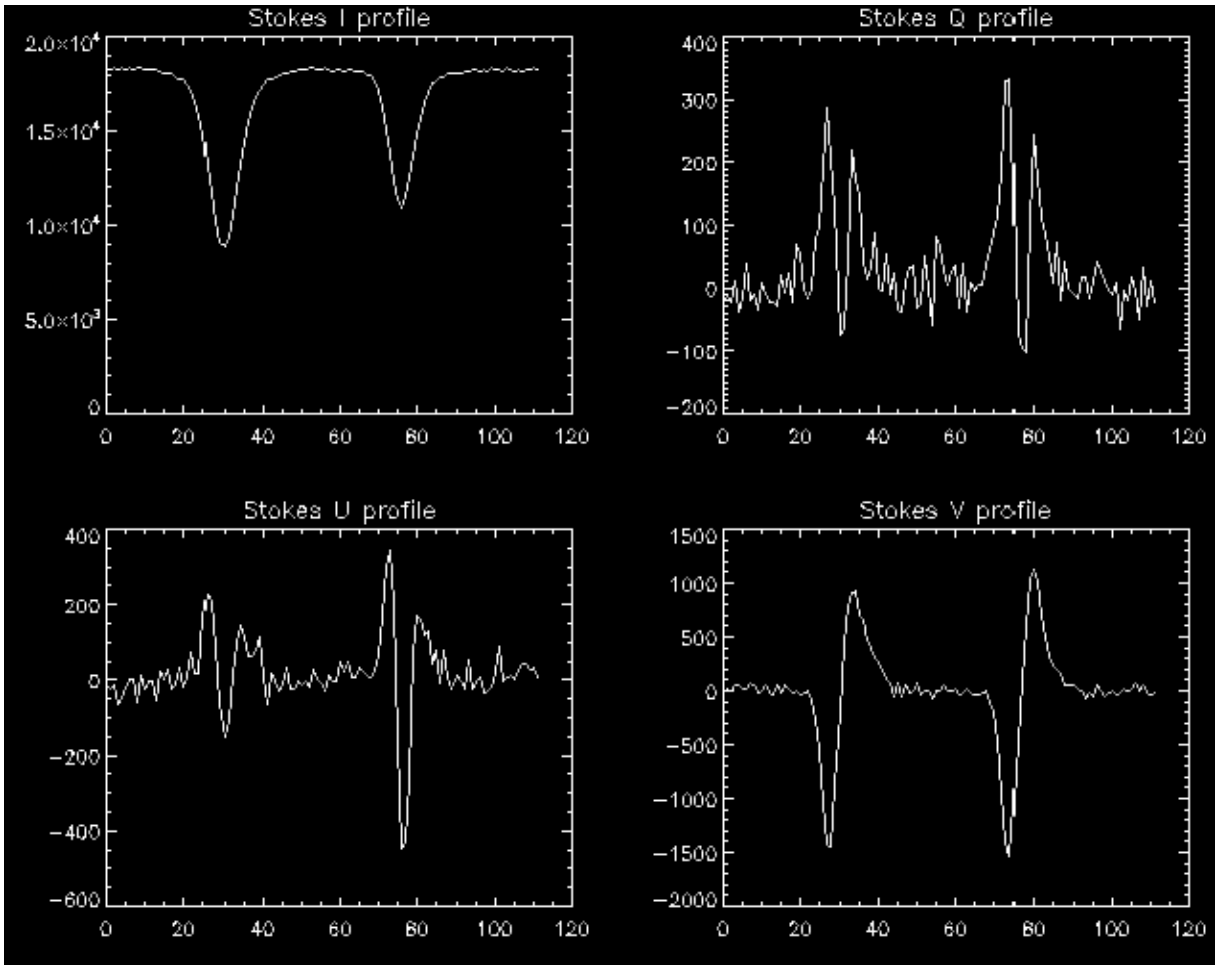

Figure 2.6: The spectrogram taken by SOT/SP. The horizontal axis is the wavelength. Unit of intensity is DN.

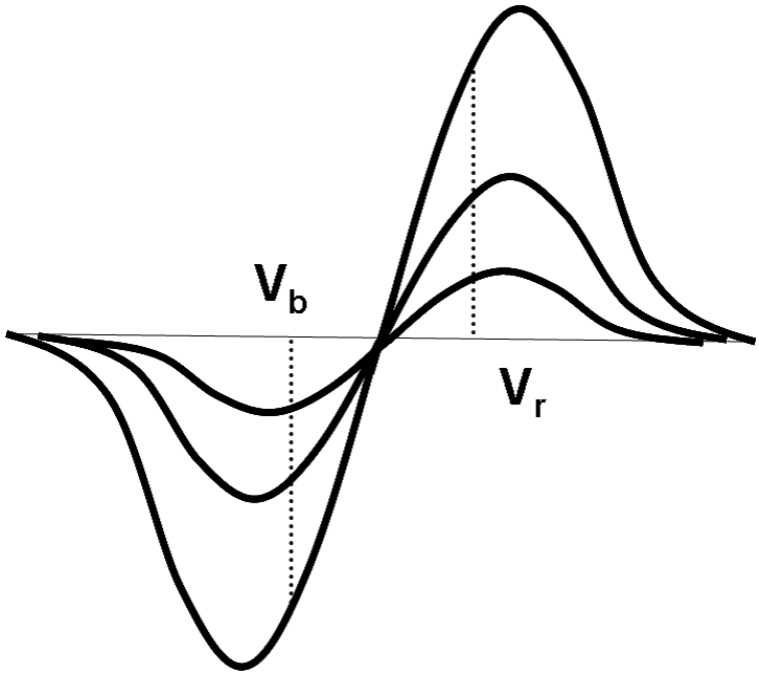

Figure 2.7: A schematic picture of Stokes-V profile. $V-b$ (V_r) is the blue (red) side of the observational wavelength. As the LOS magnetic field becomes stronger, the amplitude of V-signal arises and $G = V_b - V_r$ becomes bigger.

2.3.1 Magnetic Fields

We investigate the magnetic field from FG and SP data. We determine the magnetic field from Zeeman splitting. We use G as an indicator of LOS magnetic field. G is defined as follows.

$$G = V_b - V_r \tag{2.1}$$

Here, V_b is an intensity of blue wing and V_r is an intensity of red wing in Stokes-V signal. Left figure in Fig.2.7 shows a schematic picture of Zeeman splitting in Stokes-V signal. As the LOS magnetic field becomes stronger, the amplitude of Stokes-V signal arises and then the absolute value of G becomes bigger. Note that G is not the actual value of LOS magnetic field strength but an indicator.

The actual magnetic field strength is derived from SP data. We derive three components of magnetic field strength from SP using Milne-Eddington fitting. Mile-Eddington fitting is one of the inversion of polarization measurement. By assumption that the source function is a linear function and other physical parameters are constant, we can obtain the various physical quantity by the inversion of polarization observation. Note that there are 180 degree ambiguity of transversal magnetic field direction in the fitting results.

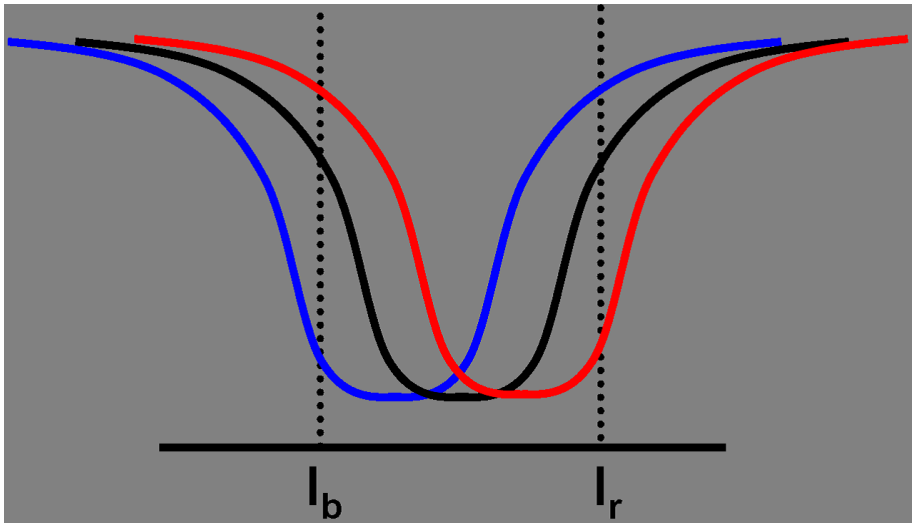

Figure 2.8: A schematic picture of Stokes-I profile with Doppler shift. Blue line, black line, and red line mean blue shift, no Doppler shift, and red shift respectively. $F = \frac{I_b - I_r}{I_b + I_r}$ becomes negative in blue shift, zero in no Doppler shift, and positive in red shift.

2.3.2 Velocity Fields

The velocity field is calculated from SOT/FG Stokes-I. We employ F as an indicator of a LOS velocity. F is defined as follows.

$$F = \frac{I_b - I_r}{I_b + I_r} \tag{2.2}$$

I_b and I_r are intensities of blue wing and red wing in Stokes-I signal. Fig.2.8 shows schematic picture of Stokes-I profile with Doppler shifts. F becomes zero if there are no Doppler shift. F is negative if there is a redshift and F is positive if there is a blue shift. We can use F as an indicator of LOS Doppler velocity. We also derive the theoretical relationship between F and an actual Doppler velocity from Atlas profile and the trancemittance spectrum of the filtergram (see Fig.2.9). We can see that a LOS velocity and F are proportional from -6.0km/s to 6.0km/s from Fig.2.9. We can say that the velocity field of cancellations are in this range according to the previous studies ($\sim$1km/s; Harvey et al., 1999; Chae et al., 2004). Doppler velocity is roughly 10 times of F in unit of km/s.

2.4 Results

The magnetic field and velocity structures of the typical cancellations are shown in this section. We found 6 cancellations in our data set. The temporal resolution of SOT/FG is $\sim$1 minute and that of SP is $\sim$20 minutes.

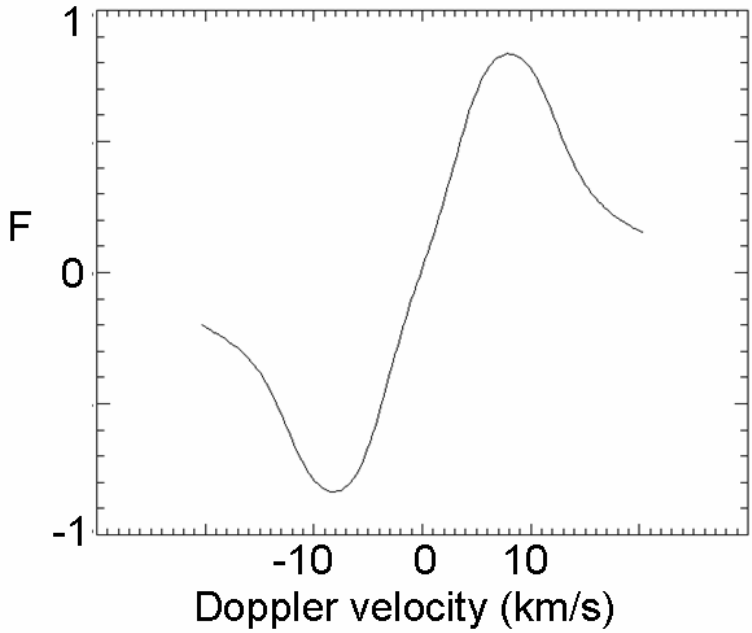

Figure 2.9: Theoretical relationship between the Doppler velocity and F. We calculate from the Atlas profile and the trancemittance spectrum of the filtergram. Doppler velocity and F are proportional.

2.4.1 Time Series of a Typical Cancellation

We determine time series of LOS magnetic field. Fig.2.10 shows time series of G. White background indicates the positive G, which means positive vertical magnetic field. Black one indicates the negative G and negative vertical magnetic field. The positive and negative patches are converging and disappearing. The negative patch disappears completely, but some parts of the positive patch remains. The time period of this cancellation is ~40 minutes. This time period is similar to the previous study (Chae et al., 2004).

2.4.2 Horizontal Magnetic Fields between canceling magnetic patches

The upper panels of Fig.2.11 show strength of the horizontal field. The gray-scale plots indicate strength of the horizontal field and the contour is the vertical magnetic field strength. Yellow contour shows positive, blue shows negative. We found that the strong horizontal field is connected when the cancellation occurs. The lower panels of Fig.2.11 show the direction of horizontal field. We can see the horizontal field between the CMFs connecting the magnetic patches. There are horizontal field connecting CMFs in 2 of the 2 investigated events..

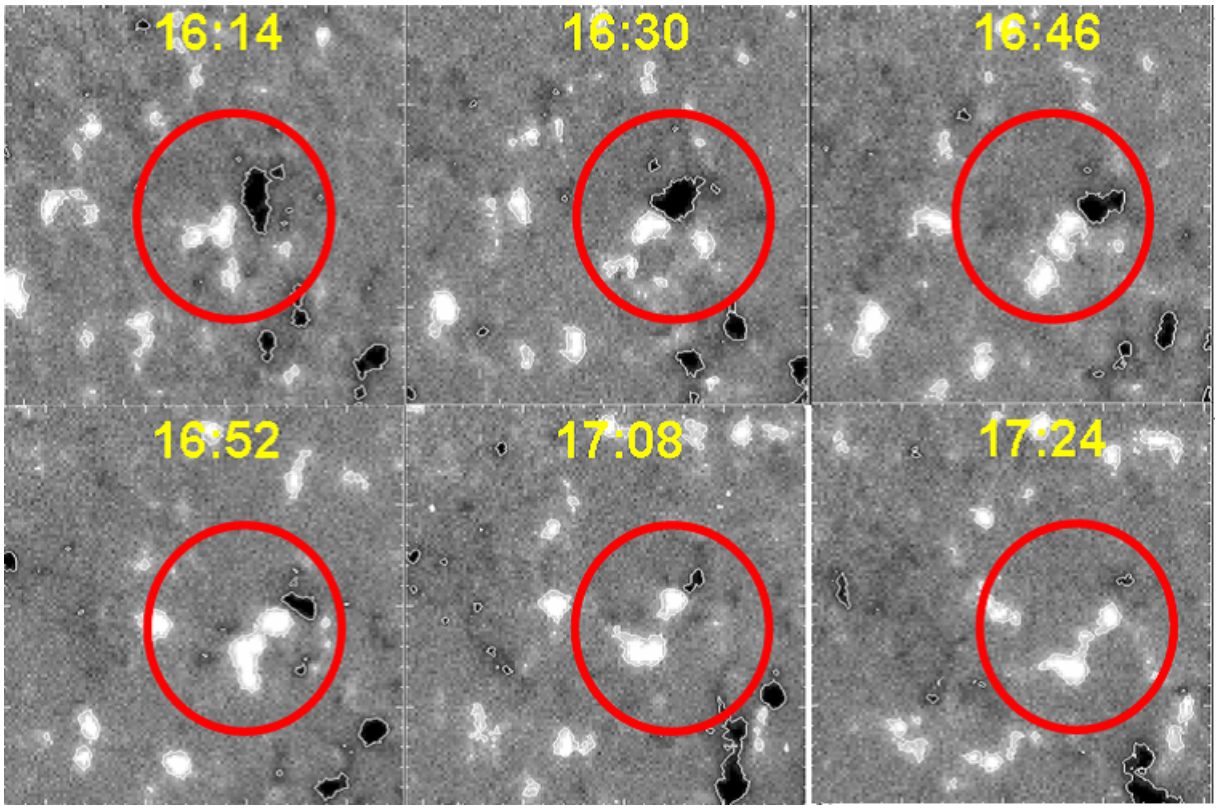

Figure 2.10: Time series of G signal (see Eq.2.1) in NaI 5869Å from SOT/FG on 2007 October 31th. The field of view is 20 arcsec × 20 arcsec.

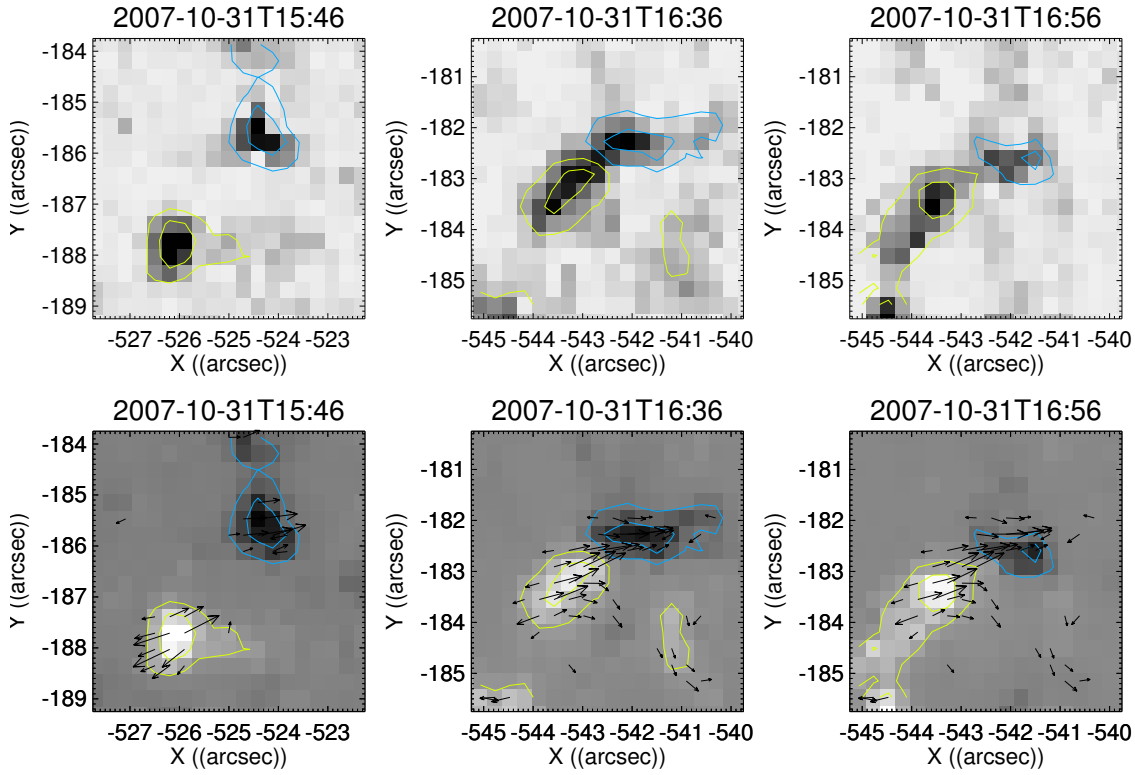

Figure 2.11: Magnetic fields obtained by the Milne-Eddington fitting of the Hinode/SP data on 2007 October 31. The maximum magnetic strength is ∼300G. The LOS component is shown in contours. Yellow (Blue) lines are for positive (negative) polarities for 100 and 300G. (Top) Magnetic strength of transversal component in gray scale map. (Bottom) Transversal component is shown by arrows. The longest arrow corresponds 300G. The transversal field between the magnetic patches is aligned as connecting each other.

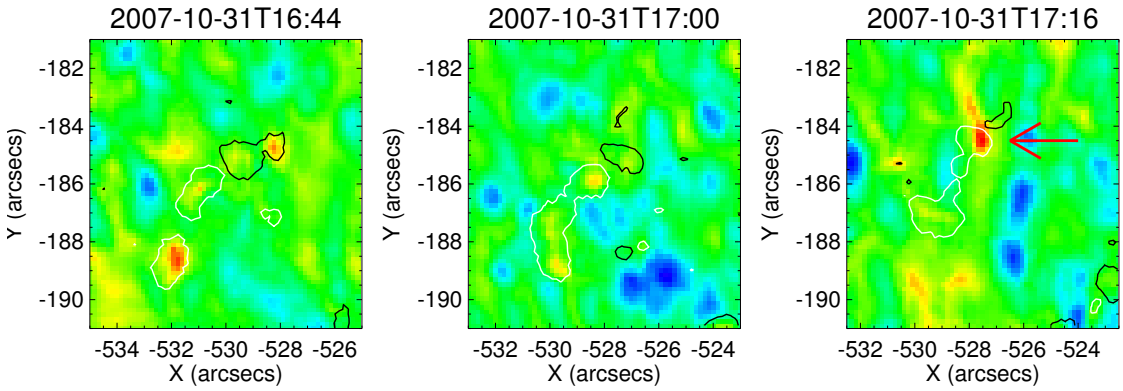

Figure 2.12: The Doppler velocity field obtained by using NaI Stokes-I from SOT/FG. The background is LOS velocity and the contour is LOS magnetic field. The red (blue) background indicates the downflow (upflow) and white (black) contour indicates positive (negative) vertical field. The field of view is 10 arcsec × 10 arcsec. The plotted range of LOS velocity is from −2.0 km/s to 2.0 km/s.

2.4.3 Velocity Fields around the Cancellation Sites

We derived the velocity field from FG data. Fig.2.12 shows the time evolution of F around the cancellation sites. The gray-scale map shows the Doppler velocity. White is downflow and black one is upflow. We found that there is a long-lasting stable downflow signature around the canceling magnetic patches. It is difficult to pick up this feature due to the ubiquitous granulation flow patterns (a few tenths of km/s with ∼one arcsec spatial scale) plus the five-minute oscillation in the Doppler images. It can be, however, discriminated since our new findings, i.e. downflow at the canceling sites, have much longer life time (∼ 40 minutes) than the granulation whose typical correlation time is ∼ 10 minutes.

We summed the Doppler velocity field over 5 minutes to see the average motion to compare the Doppler velocity around the cancellation to the other granular motions. Fig.2.13 is a Doppler field summed over 5 minutes. We can see the downflow velocity at the cancellation sites. But the downflow velocity seems a more characteristic feature in its strength and long life time. Downflows in the magnetic patches are larger than those outside the magnetic patches as in Fig.2.12. They have larger speed (∼1.0km/s). On the other hand, downflows outside the magnetic patches are less than 0.5km/s. Concerning about the velocity field around the magnetic patches, there are strong downflows both in the CMFs and non-CMF magnetic patches. We can see that the downflows in the CMFs are more stable than those in non-CMF magnetic patches. The downflow in the CMFs remains ∼40 minutes. However, downflows in non-CMF magnetic patches remain less than 10 minutes. The downflow around the cancellation site is characteristic in the velocity strength and its stability. We can observe such characteristic downflows in 5 events / 6 events.

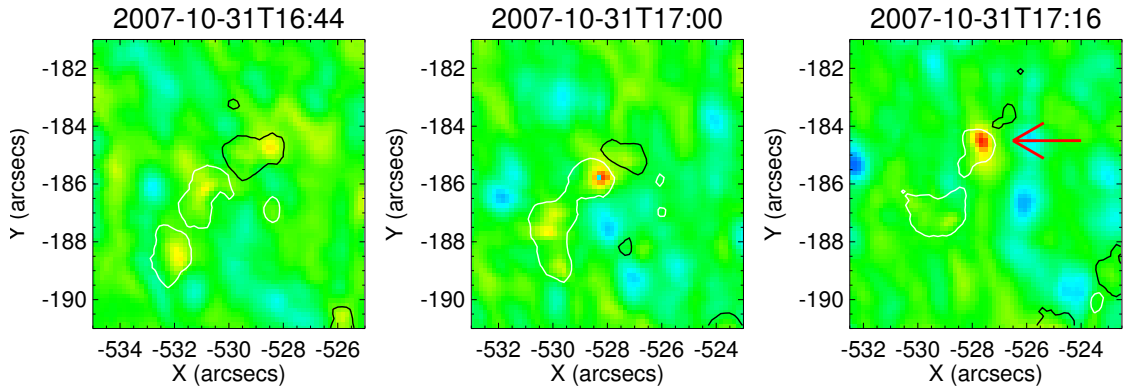

Figure 2.13: The Doppler velocity field summed over 5 minutes from SOT/FG. The background is LOS velocity and the contour is LOS magnetic field. The field of view and colors are same as Fig.2.12. The plotted range of LOS velocity is from −2.0 km/s to 2.0 km/s.

2.4.4 Time Series of the Magnetic Flux and Velocity Structures

We checked the time series of the magnetic flux and velocity field. Fig.2.14 shows the integrated V-signal time series in a cancellation site. The solid line shows time series of positive V-signal and the dashed line shows that of negative V-signal. We can see the cancellation occurs around 16:42 and the negative patch disappears at 17:20. We can see that the downflow at the cancellation site is not clear before the cancellation in Fig.2.13. There is a characteristic downflow during the cancellation and the downflow disappears after the cancellation. The doppler velocity is in the CMFs at first but it moves toward the gap of the CMFs.

2.5 Discussions

Our results of the typical cancellation is as follows:
(1) The strong horizontal field between CMFs are observed during the cancellation.
(2) The direction of the horizontal field is aligned to connect the CMFs.
(3) Characteristic downflows are dominant at the cancellation sites.
We discuss the cancellation scenarios in this section based on these results.

2.5.1 Horizontal Magnetic Fields Connecting the CMFs

We observed horizontal magnetic fields connecting CMFs in 2 events / 2 events. The horizontal field at the cancellation sites is reported in two papers (Chae et al., 2004; Kubo et al., 2007). These two papers report the horizontal field. There are no reports on the direction of the horizontal field in Chae's paper. Kubo reports that the direction of the horizontal field at the cancellation sites is aligned to the polarity inversion line between the canceling polarities. But his cancellations are in the active regions and there are filament formations around

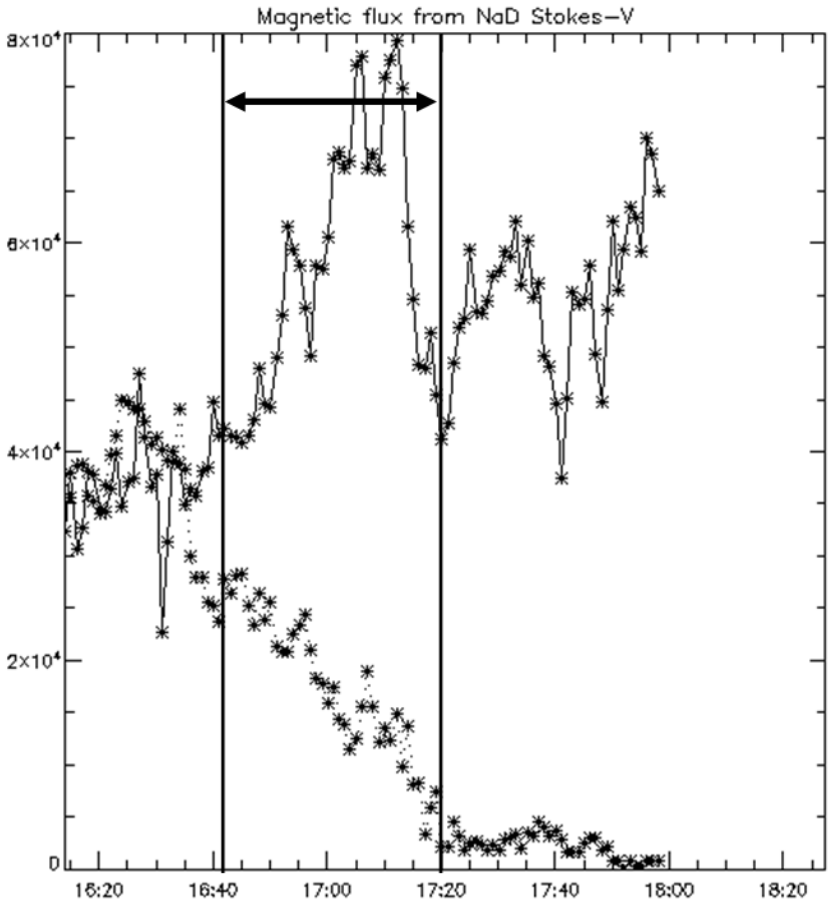

Figure 2.14: The time evolution of magnetic flux of the cancellation. We integrate Stokes-V around the cancellation site. The solid (dotted) line is positive (negative) flux. The cancellation occurs between 16:42 to 17:20.

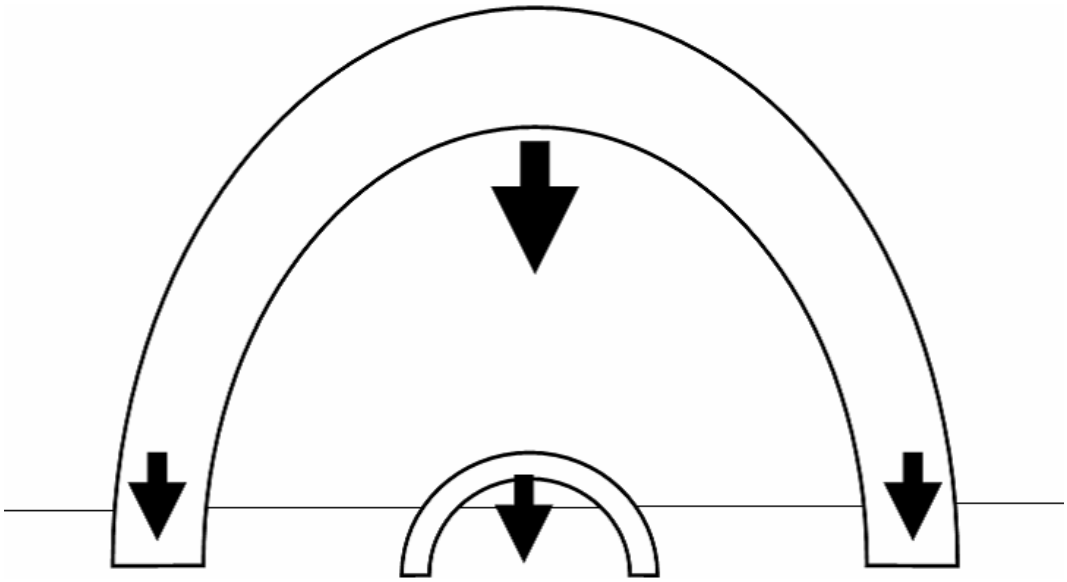

Figure 2.15: A schematic picture of Ω-loop submergence. The downflow can be seen at the footpoint of Ω-loop at first and in the same position with the horizontal field later.

his cancellations. Our analysis is the first one to determine the directions of quiet region cancellations.

The horizontal magnetic field is a necessary condition both for "U-loop emergence" and "Ω-loop submergence" scenarios. We should see horizontal field when the U-loop just emerges from below the photosphere or Ω-loop just submerges from above the photosphere. The horizontal fields in our observations are consistent with these scenarios in this point.

On the other hand, it is difficult to conclude which scenario is dominannt only by magnetic observations at this moment (although it became possible by the Doppler measurement. See the next section.). Horizontal field is aligned from a negative patch to a positive patch at the photosphere in U-loop. On the contrary, horizontal field is aligned from a negative patch in Ω-loop. However, there is 180 degree ambiguity in the determination of the transversal azimuth angle by the fitting method for the spectropolarimetric data based on the Zeeman effect.

2.5.2 Dominant Downflow around the Cancellation Sites

Strong and long-lasting downflows are observed in 5 events / 6 events. We think these characteristic downflows are evidences of "Ω-loop submergence". The time series of velocity structures can be obtained because we can derive the Doppler velocity from filtergram data. Fig.2.15 shows a schematic picture of "Ω-loop submergence" scenario and expected velocity structure. Time evolution of the downflow position is consistent with our observations. This fact supports the "Ω-loop submergence" scenario.

2.5.3 An Estimation of the Submerged Magnetic Flux

We estimate the magnetic flux (Φ_1) when the magnetic patches are isolated and the submerged flux (Φ_2) with the assumption that the magnetic field is subtracted with the observed downflow velocity. If the downflow is the actual submerging velocity, these fluxes will be equivalent. Φ_1 is calculated as follows,

$$\Phi_1 = B_{LOS} \times S \tag{2.3}$$

Here, B_{LOS}, S are a LOS magnetic field strength, an area of a magnetic patch when it is isolated enough. B_{LOS} is obtained by Milne-Eddington inversion of SP and S is from the SP Φ_2 is calculated as follows,

$$\Phi_2 = B_{hor} \times l \times v \times t \tag{2.4}$$

By using $B_{LOS} = 200G$, $B_{hor} = 200G$, $t = 20min$, $v = 2.0km/s$, $l = 1arcsec$ we obtain $\Phi_1 = 5.0 \times 10^{18}$Mx, $\Phi_2 = 3.5 \times 10^{18}$Mx. These values are almost equivalent.

2.5.4 What is the "Ω-loop submergence" mechanism?

We conclude that the observed cancellation is a "Ω-loop submergence". What is the "Ω-loop submergence" mechanism? It is difficult for an Ω-loop to submerge due to the magnetic buoyancy. The key point is a length scale in which the downflow is observed. The magnetic buoyancy becomes the same order of magnitude as to the magnetic tension if the length scale is a few times of pressure scale height. The pressure scale height is ∼250km at the photosphere. We can know the length scale from SP or FG data and the length scale of the downflow is ∼ 1arcsec=730km (see Fig.2.11).

The magnetic buoyancy is not superior to the magnetic tension in this length scale. Based on these discussions, we speculate the "Ω-loop submergence" scenario (see Fig.2.16). First, the magnetic flux tubes are convected by the supergranulation. These magnetic flux tubes are not connected. When the magnetic flux tubes are at a short distance, it reconnects above the photosphere. The foot-points of the magnetic fluxes continue to converge. Finally, when the magnetic patches are at a short distance enough, the magnetic tension of the new magnetic field is larger than the magnetic buoyancy. Then, the newly formed "Ω-loop" begins to submerge. In this scenario, the main cause of the submergence is magnetic tension of the magnetic flux tube.

2.6 Summary and Future Works

We obtain the temporal evolution of velocity and magnetic structures of quiet region cancellations by using *Hinode* observations. It is the first time to investigate the velocity and magnetic structures of quiet region cancellations by direct observations and time evolution of velocity structures. We found the horizontal fields connecting the canceling magnetic patches. This

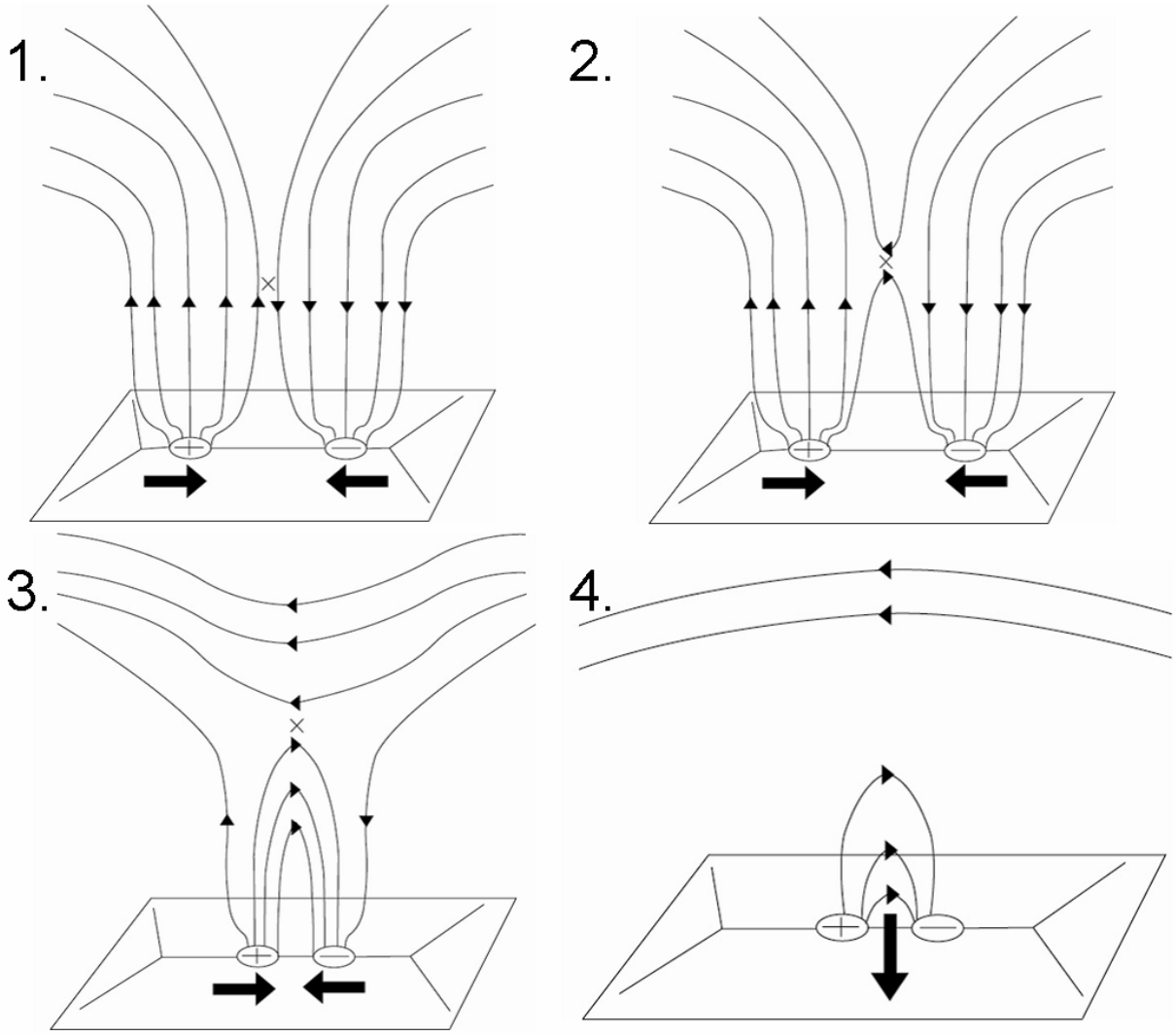

Figure 2.16: Schematic pictures of a cancellation scenario. Two magnetic flux rope are convected by the supergranultaion. When they get close, a magnetic reconnection happens in the solar chromosphere or corona. They continue to converge after the reconnection. The newly formed magnetic fields submerge by magnetic tension when they get closer than a few times of scale height.

result is different from the previous study of active region cancellations accompanying filament formations. We also found the strong and stable downflows at the connecting sites. We also the temporal evolution of the velocity field and check the consistency between the isolated flux and the flux. From these results, we conclude that the observed cancellation is an "Ω-loop submergence".

In the future, we will apply the same analysis to the other data sets to determine the generality of characteristic structures. We have to statistically investigate the magnetic field and velocity field. According to this study, we can investigate the cancellations in quiet regions. There are 35 cancellations in *Hinode* data from October 2006 to August 2008. This is enough to study the structure of the cancellations statistically. We also want to investigate the spectra of the cancellations in more detail because the field of view of SOT/SP can be selected. The temporal resolution of becomes higher as the field of view is smaller. The difficulty of this observation is whether there are some cancellations or not in the field of view. The investigations of XRT and EIS at the cancellation sites are also needed. If the magnetic reconnection occurs in the chromosphere or the corona, XBP and/or EUV bright point should be observed. We may observe some velocity structures by analyzing EIS. These are very important and interesting investigations in the future.

Chapter 3

Association between the Cancellations and the Filament Formations

3.1 Introduction

Filament consists of cool materials and its density is higher than its circumstances (Hirayama, 1985, see Fig. 1.5). Its materials will fall down by gravity without an additional force. However, some filaments keep their configuration for some months (Martin et al., 1998). Some authors found that filaments are along the polarity inversion line, PIL (Babcok & babcock, 1955; Howard et al., 1959; Martin et al, 1998). This shows magnetic field plays an important role of its existence. Magnetic field of filaments was determined by Leroy et al. (1989) and various magnetic fields are proposed, which can keep its materials against gravity (Martin et al., 1998; Kuperus & Raadu, 1974; Kippenhahn & Schlüter, 1957). Though magnetic configuration of filaments are debated and its configuration near the photosphere is observed in recent observations (Lites et al., 2005; Lòpez Ariste et al., 2006), its actual configuration has not been determined.

The filament formation gives some clues to its magnetic configuration. From an observational point, a convergence (Martin et al., 1990) and a cancellation (Livi et al., 1985; Martin et al., 1985; Wood & Martens, 2003; Schmieder et al., 2006) of photospheric magnetic patches are observed during a filament formation. A lot of formation models are proposed, satisfying these observations that there are convergences and cancellations of the photospheric magnetic patches during the filament formations. They can be divided into two categories. One is a flux emergence model (Rust & Kumar, 1998) and the other is a reconnection model (van Ballegooijen & Martens, 1989; Martens & Zwaan, 2001).

In Rust and Kumar model (see Fig.3.1), a convergence and a cancellation of magnetic patches are resulted when the ”U”-like undulated part of a flux emerges. We can see a convergence and a cancellation on the photosphere when flux emerges from below the photosphere. Filaments are formed by emerging of flux below the photosphere. In this model, canceling magnetic patches must be connected under the photosphere. Martens and Zwaan model (Head-to-tail linkage model) explains convergences and cancellations on the photosphere as a reconnection in the photosphere. Note that it does not matter whether the magnetic field is

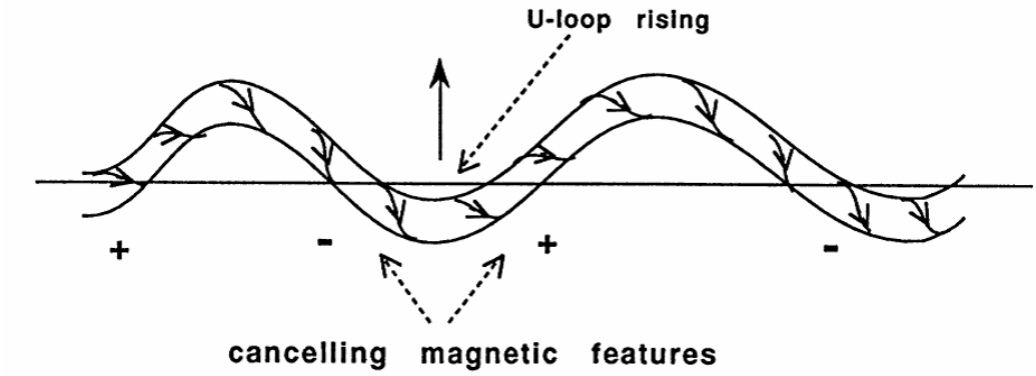

Figure 3.1: The flux emergence model from Zwaan (1987). We can see the vertical magnetic patches converge at the photosphere when the magnetic flux emerges from below the photosphere.

connected under the photosphere or not. Martens and Zwaan said that repeated reconnections in different positions make twisted magnetic field (see Martens & Zwaan 2001, see Fig.3.2) and the magnetic field line has dips along their field line. It is confirmed by a numerical simulation that the magnetic configuration is made as theoretically expected by reconnections (Welsch et al., 2005; Litvinenko et al, 2005).

There are two types of filaments, an active region filament and a quiescent filament. An active region filament is in or near the active region. A quiescent filament is far from active regions. There are not only similarities but also differences between them. Both are along the PIL (Babcock & Babcock, 1955; Howard et al., 1959). Convergences and cancellations are observed in both filaments (Livi et al., 1985; Martin et al., 1985; Martin et al., 1998). However, typically active region filaments have shorter bodies, act violently as their name. Their life time is shorter than quiescent filaments'. On the other hand, quiescent filaments have longer bodies, and look less active. Their life time is longer than active region filaments (Martin et al., 1998). They sometimes live for more than a month. There are more morphological differences between them about barbs and hemispheric patterns (Martin, 1998). Quiescent filaments seem to have more barbs along their side than active region filaments. Quiescent filaments show hemispheric patterns, but active region filaments do not show (Martin et al., 1994; Martin et al., 1998). Martens and Zwaan theoretically explained barbs and its hemispheric pattern by Head-to-tail linkage model. These fact may indicate the difference of magnetic configurations and/or formation processes between quiescent and active region filaments.

These filament formation scenarios are difficult to distinguish by observations of photospheric magnetic field because both of them are based on the fact that a cancellation is a necessary condition for a filament formation. On the other hand, most of the cancellations are associated with the EUV brightening (Harvey et al., 1999). If the magnetic reconnection occurs when the filament is formed, an EUV brightening should be observed. But few papers

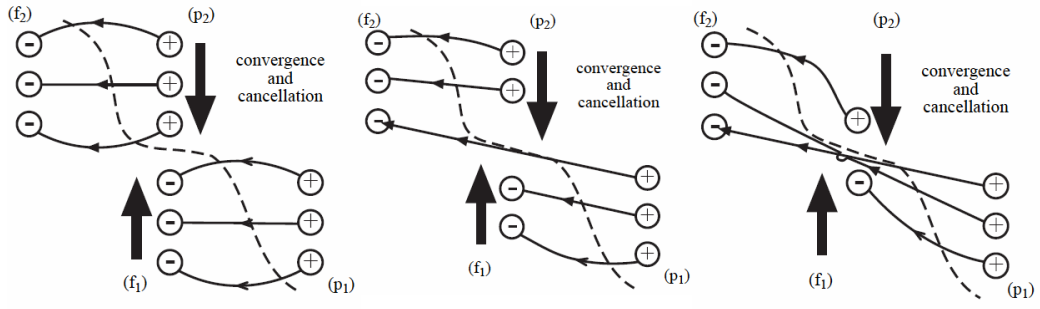

Figure 3.2: The Head-to-linkage model from Martens & Zwaan (2001). The dotted line is the polarity inversion line at the photosphere. There are photospheric cancellations when the magnetic reconnection occurs.

report the association of the filament formations and EUV brightenings. We think the EUV brightenings are important evidences for filament formations by reconncetion models. Note that a recent study strongly indicate that the flux emergence occurs when an active region filament is formed (Okamoto et al., 2008). However, we should determine the association between cancellations and filament formations in the quiet regions addition to the active regions.

We investigate the association of cancellations, filament formations, and EUV brightenings in this study. Our purpose of this study is to determine the filament formation models, namely a flux emergence model and a reconnection model. Full-disk Hα images, line-of-sight (LOS) magnetic field images, and EUV images are used for statistical analysis. We used Hα images taken by SMART/Hida Observatory, LOS magnetic fields images by SOHO/MDI, and EUV images by SOHO/EIT. These instruments take full-disk images. In section 2, we describe the instrumentations. Detection criteria in this study for cancellations, filament formations, EUV brightenings and simultaneous events are given in section 3. The results are shown in section 4. These results are shown about active region and quiet region respectively. We made some discussions in section 5. The adequacy of the flux emergence model and the reconnection model is especially discussed. The conclusion and the future works are shown in section 6.

3.2 Instrumentation

We briefly introduce the instrumentations in this section. Hida/SMART, SOHO/MDI and SOHO/EIT are used in this study.

We use Hα images taken by Solar Magnetic Activity Research Telescope (SMART). Filaments are observed clearly in Hα images. SMART is in operation at Hida Observatory, Kyoto University. SMART can take a full-disk Hα line-core and Hα wing (0Å,±0.5Å, ±0.8Å) images every a few minutes. It has 2 arcsec spatial resolution (Ueno et al., 2004). This spa-

tial resolution is enough to detect filament formation of the main body. Because we can see all the filaments on the disk thanks to full-disk images, they enable us to determine filament formations statistically.

SOHO (Solar and Heliospheric Observatory) is a solar observation spacecraft launched in 1995 by NASA and ESA. MDI is one of the instruments aboard SOHO. MDI takes full-disk LOS magnetograms every 96 minutes, which we use to determine cancellations on the photosphere. Because a typical cancellation continues for six hours or more, we think the temporal resolution is enough to determine cancellations. MDI magnetogram's noise level is 20 Gauss (Scherrer et al., 1995). We can clearly see the magnetic patches more than 25 G. We also use full-disk 195Å EUV images taken by SOHO/EIT. We use 12 minutes EUV images. The spatial resolution is 4 arcsec/pix. We can determine EUV brightenings statistically with full-disk EUV images.

3.3 Analysis

In this section, we define the detection criteria for a filament formation, a cancellation, and an EUV brightening. We determine the simultaneity of a filament formation, a cancellation, and an EUV brightening from these definitions.

3.3.1 Event Selection

We define a filament as a dark line in the Hα images by visual inspection. We want to determine formations, namely large change of the length of filament spines. Filament's length is defined as the length along the filament spine. The length is the longest line of a filament and nearly along the PIL.

A filament is called an active region filament if a part of the filament is in 100 arcsec from the nearest active region in this study. On the contrary, a filament is called a quiescent filament if there is no active regions in 100 arcsec from the filament.

We selected filaments which are located in $-600arcsec < x < 600arcsec, -600arcsec < y < 600arcsec$ in the solar coordinate. This is because to avoid the projection effect for the determination of the vertical magnetic field against the surface based on the observed LOS component. In addition, we select filaments whose spines are longer than 100 arcsec. Some active region filaments are shorter than 100 arcsec and these short filaments are removed from our target. We investigate the configuration of the large active region filaments. Large filaments are thought to live longer (Martin, 1998). SMART is affected by the weather and there are some days in which Hα images can not be taken. We chose filaments which is successively observed for more than three days. There are 24 active region filaments and 29 quiescent filaments satisfying the above conditions.

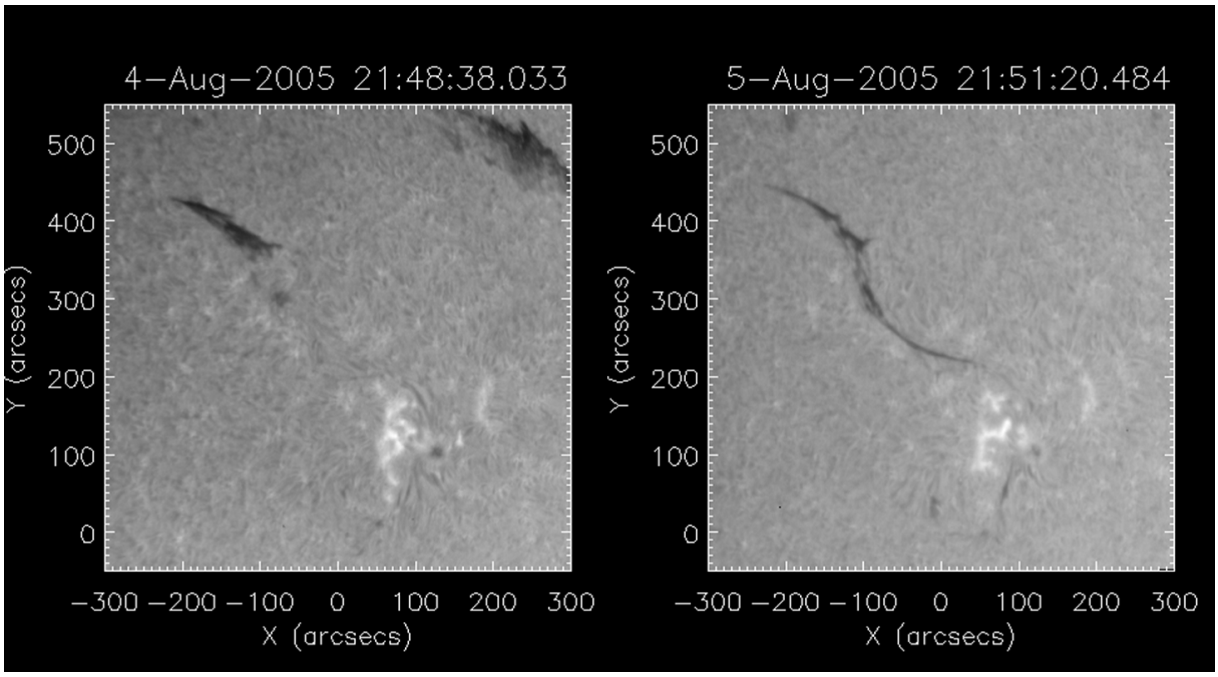

Figure 3.3: An example of filament formations. We can see the filament formation more than 50 arcsec. These images are from SMART/Hida Observatory.

3.3.2 Detection criteria of Filament Formations

Filament formations are defined as follows: (1) A new appearance of a filament longer than 50 arcsec. (2) The linkage of dark filaments which are not connected before. (3) The lengthening of a filament spine by longer than 50 arcsec. The 50 arcsec is long enough to observe the filament's change clearly. We determined the apparent filament's spine formations. We count a continuous filament formation as one filament formation. The period during which the filament is is defined a filament formation period. Fig.3.3 is an example of filament formations. SMART can not take Hα images during night, but some filaments are formed during night. We count such filament formations, too.

3.3.3 Detection criteria of Cancellations

The detection criterion for cancellations is given by the amount of the unsigned LOS magnetic flux Φ of each canceling patch. The threshold is given as $\Phi > 10^{19} Mx$. This value is given by the crude requirement for the support of the newly-formed filament's material against the gravitational fall. [A typical filament width (w), filament height (h), and magnetic field of the spine (B_c) are 1.0×10^9 *cm*,1.0×10^{10} *cm*, and 10 G respectively (Aschwanden et al., 2004; Leroy et al., 1989). Typical flux of a filament (Φ) is estimated as $\Phi \sim h \times l \times B_c \sim 10^{19}$ Mx.] This threshold value is also used by the previous studies (Martin et al., 1994; Wood & Martens, 2003). Note that there are cases in which the cancellation occurs between both

isolated positive and negative patches as well as between patches one of which are not-well isolated from the background fields. Even in the latter case, one of the patch should be isolated for the detection here and the criterion is applied to this isolated patch. To avoid the instrumental noise (~20G), the magnetic flux of each patch is measured as a sum of the fluxes of the data pixels in which the LOS magnetic strength is greater than 25G. It can be said that MDI has enough spatial resolution. The other cancellation is a continuous cancellation. In this cancellation, positive and negative magnetic patches conflict each other. However, they can not be distinguished from the other magnetic patches because the cancellation occurs too near active regions or plage. Such a confliction is usually observed near an active region filament. The magnetic flux decrease can not be determined if magnetic patches can not be distinguished. In this case, if positive and negative magnetic regions get away each other, we count as a cancellation. Note that we determine long lived active region filaments. In or near the center of an active region, the change of a magnetic flux can not be distinguished, because magnetic flux may rise from under the active region. But active region filaments in this study are not at the center of an active region because filaments tend to be shorter in such a region.

3.3.4 Detection criteria of EUV Brightenings

We define the EUV brightening as the increase of the intensity. Quiescent filaments are usually located at the dark region in EUV images. We can see an EUV brightening around the quiescent filaments. On the contrary, active region filaments are near or in the active region. It is difficult to see an EUV brightening in a very active region because the EUV intensity of an active region is near the saturation. We, therefore, did not use such data for our statistical countings of the association of EUV brightenings with filament formations.

3.3.5 Comparison of Filament Formations, Cancellations, and EUV Brightenings

We investigate the simultaneity of these activities. The target cancellations and EUV brightenings are searched along the filament spines. We say a filament formation and a cancellation is simultaneous if the formation and cancellation occur at the same place and have overlapping in the time series. Active region filaments and quiescent filaments are investigated separately because it is possible that filaments are formed in different processes in different regions.

3.4 Results

3.4.1 Filament Formations and Simultaneous Cancellations

Fig.3.4 shows the simultaneous events of a filament formation and a cancellation. Upper panels show the LOS magnetic field. We can see a cancellation in these images and note that

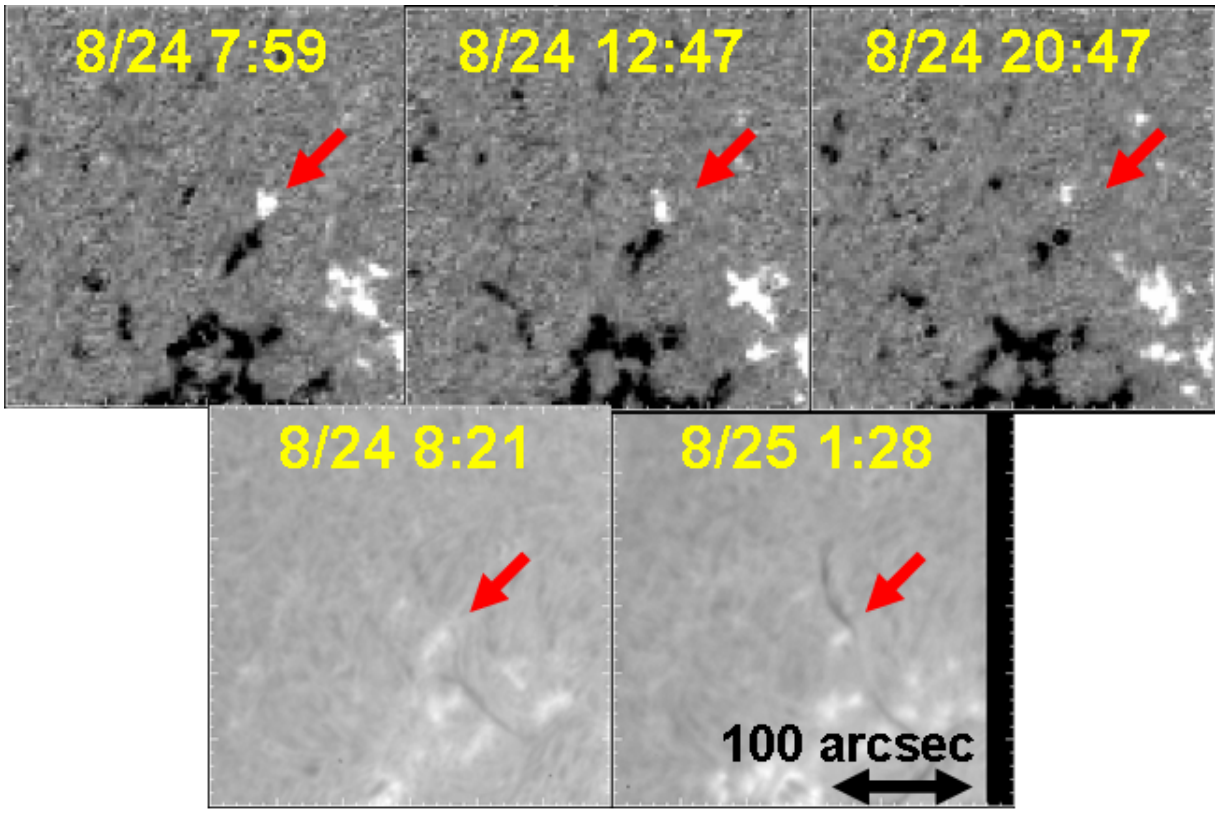

Figure 3.4: A simultaneous event of filament formation and a photospheric cancellation.

cancellation occurs at the filament extension point. Lower panels are Hα images in the same field of view. We can see a dark filament and its extension.

There are also filament formations without photospheric cancellations. Fig.3.5 is an example of filament formations without photospheric cancellations.

3.4.2 Filament Formations and Simultaneous EUV Brightenings

The panels in Fig.3.6 show EUV images of the same cancellation of Fig.3.5. The field of view is the same as Fig.3.5. We can see an EUV brightening which occurs at the place where the filament formation occurs. We can not see EUV brightening at 0:00, the right figure in the upper line. The brightness of EUV images is gradually increasing from 4:36. In the next panel, we can see the clear EUV brightening. We can see the filament is above the EUV brightening, too. Between 14:00 and 18:24, the filament are growing above the EUV brightening from the north to the south. EUV brightening occurs earlier than the filament formation. This EUV brightening are observed until the next day. We notice that there are some magnetic patches near the EUV brightening point comparing with the magnetic field of Fig.3.5. The characteristic points are the time series between the EUV brightening and the filament formation, the filament is overlying the EUV brightening, and the existence of the magnetic patches.

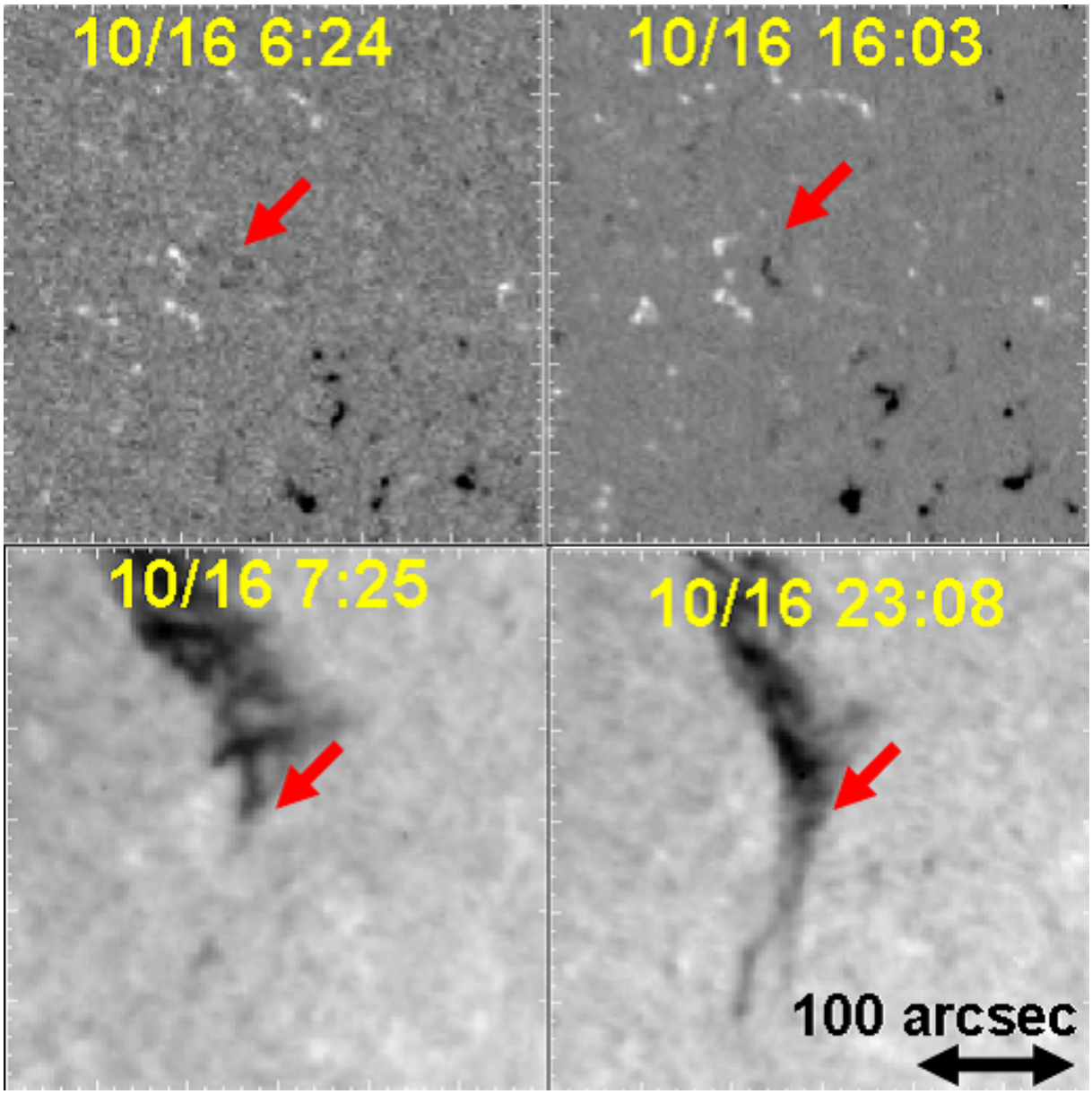

Figure 3.5: A filament formation without photospheric cancellations. The arrows indicate the formation point.

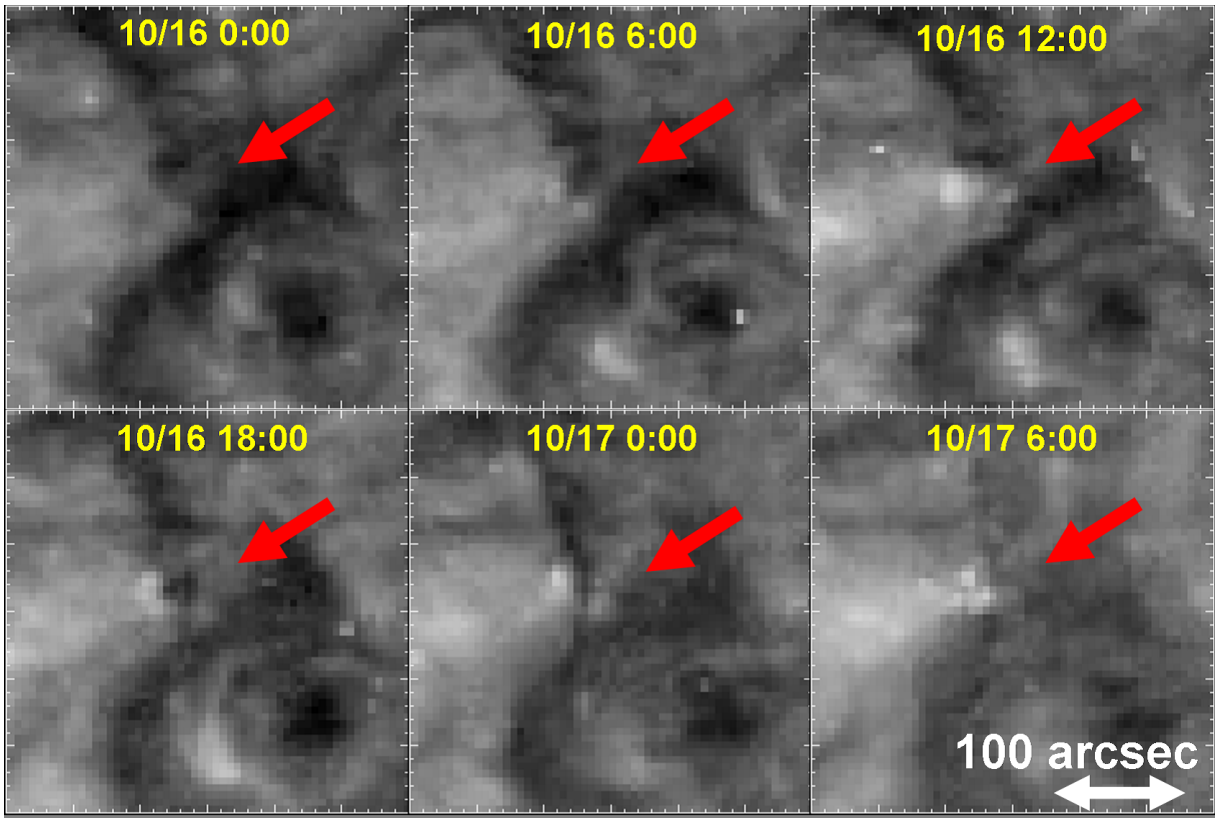

Figure 3.6: EUV images of a filament formation without cancellations. The arrows indicate the EUV brightening. We can see a filament formation in EUV images.

The fact that the EUV brightening is observed earlier than the filament formation meets that filament materials are formed after the magnetic loops supporting materials are made by the photospheric-above reconnections. The next characteristic that the filament overlies the EUV brightening is expected if reconnections occur like the Head-to-tail linkage model.

3.4.3 Statistical Results

In this section, we show the statistical result. The result of active region and quiet region are shown respectively.

Table 3.1 shows numbers and ratios of simultaneous events and filament formations without cancellations. The first line is those of 24 active region filaments and the third line is those of 29 quiescent filaments. 17 simultaneous events and 15 filament formations without cancellations are observed in the active regions. There are more filament formations without cancellations than simultaneous events. The ratio of simultaneous events is 53%. About half of filament formations in active regions are associated with cancellations. However, some filament formations in active regions are not associated with cancellations. 7 simultaneous events and 14 filament formations without cancellations are observed in quiet regions. The

	Filament formations with cancellations	Filament formations without cancellations
Active Regions	17 events (53%)	15 events (47%)
Quiet Regions	7 events (33%)	14 events (67%)

Table 3.1: The ratio of filament formations with cancellations.

	cancellations and EBPs	cancellations but no EBPs	no cancellations but EBPs	no cancellations and no EBPs
Active Regions	7 events (28%)	7 events (28%)	2 events (8%)	9 events (36%)
Quiet Regions	5 events (33%)	0 events (0%)	6 events (40%)	4 events (27%)

Table 3.2: The ratio of EUV brightenings to filament formations.

ratio of simultaneous events is 33%. We can say that about one third of filament formations are associated with cancellations. But many filament formations are not associated with cancellations. The ratio of the filament formations without cancellations is bigger than that of active regions. In both active regions and quiet regions, we observed some filament formations without cancellations.

Table.3.2 shows the result of simultaneity of filament formations and EUV brightenings. There are no EUV images in some filament formations and the total number of filament formation decreases. In active regions, there are 9 EUV brightenings associated with filament formations. About one third of filament formations are associated with EUV brightenings. Half of the simultaneous events are associated with EUV brightenings. We can notice that the ratio of the EUV brightenings associated with filament formations is larger in quiet regions. There are 11 EUV brightenings associated with filament formations. The ratio of filament formations associated with EUV brightenings is 73%. All of the simultaneous events are associated with the EUV brightenings and more than half of filament formations without cancellations are associated with EUV brightenings.

3.5 Discussions

In the previous section, we found
(1) There are filament formations without cancellations in both active regions and quiet regions. (Table.3.1)
(2) The ratio of filament formations is larger in quiet regions than in active regions.
(3) The ratio of EUV brightenings to the filament formation is larger in quiet regions than in

active regions.
We discuss the filament formation scenarios in this section. Based on these findings, we discuss the mechanisms of a filament formation, by using the proposed two main models, i.e. the flux emergence model (e.g. Rust & Kumar) and the reconnection model (e.g. Martens & Zwaan) as guidelines for the discussion. The difference in the mechanisms between the quiescent and active-region filaments are also discussed.

3.5.1 Filament Formations and Cancellations

We found that there are some filament formations without photospheric cancellations in both active regions and quiet regions. This might be a supporting evidence for the reconnection model because of the following reasons. We think a photospheric cancellation should be observed if the flux rope emerges from below the photosphere. If a filament is consist of a magnetic flux tube, the possibility of weak field strength during the emergence is unlikely since the expected strength is more than the detection limit (~25G) of MDI according to the crude estimation of the required strength for a filament material to be supported against the gravity. Magnetic field necessary for supporting typical filament material against the gravity is 10 Gauss in the corona. We think the magnetic field which consists a filament can be detected in the MDI image if a flux rope emerges from under the photosphere. This is because the magnetic field is stronger in the photosphere than in the corona according to the external pressure. On the other hand, if the filament magnetic structure is generated by the reconnection far above the photosphere, i.e. in the chromosphere or in the corona, then the canceling feature is not required in the magnetograms. Note that if a filament is consist of flux tubes thinner than the MDI resolution, it is possible that we can not see the thin flux tubes because the Zeeman effect is canceled with mixed polarities.

3.5.2 Filament Formations and EUV Brightenings

We may use the simultaneous EUV observations to check the idea of the non-photospheric reconnection suitable for the filament formation mechanism. If the reconnection is occurring in the transition region or in the corona, a brightening should be associated with the Hα filament formation. Magnetic reconnections like the Head-to-tail linkage model will produce magnetic dips in upper loops. Additon to this, magnetic reconncetions in the Head-to-tail linkage model should result in the existence of the magnetic patches near the EUV brightening point. These remnant are the lower loops produced by magnetic reconnections. It is possible that the lower loops can not submerge and the magnetic field of the filament footpoint does not change because of the magnetic buoyancy. Note that it is also possible that an "Ω-loop submergence" occurs after reconnections in the solar atmosphere. If downward motion produced by the reconncetion outflow is large enough to submerge through photosphere. In fact, some cancellations are determined as a submerge of magnetic field (Harvey et al., 1999; Kubo et al., 2007). We do not know the condition to submerge through photosphere yet. But we think the EUV brightening is supporting magnetic reconncetion models in the solar atmosphere.

3.5.3 Filament Formation Models

We discuss the different ratio of simultaneous events to filament formations without cancellations between active regions and quiet regions. In active regions, 53% filament formations are associated with photospheric cancellations. On the other hand, only 33% filament formations are associated with photospheric cancellations in quiet regions. The ratio in active regions is larger than in auiet regions. Addition to this, the ratio of EUV brightenings is larger in the quiet regions than in the active regions. More over, the ratio of the EUV brightening in quiet regions is larger than in active regions. We speculate that the different process of filament magnetic field's formation produces this difference. In active region, the process of a filament formation is a flux emergence. On the other hand, the main process is reconnection model in quiet regions. A recent study strongly shows an active region filament is formed by a flux emergence (Okamoto et al., 2008).

3.6 Summary and Future Works

We investigated the association of photospheric cancellations, filament formations, and EUV brghtenings. There are filament formations without cancellations both in active regions and quiescent regions. We speculate a filament formation without filament formation is possible by reconnections in the chrmosphere or corona. The association of filament formations and EUV brightenings supports this speculation. There are EUV brightenings in filament formations wihtout cancellations. Addition to statistical results, we can see filament formations in EUV images after the brightenings. This strongly supports the filament formations by reconnections in the solar atmosphere.

But there is a possibility that a filament consists of many thin flux tubes. This possibility is testified by observations of higher resolutions, for example, *Hinode* SOT. Unfortunately it is a solar minimum and there are few filaments on the solar disk. It is difficult to observe filament formation with high temporal and spatial resolution because there are no signatures of a filament formation and higher resolution means smaller field of view. But it is important to investigate the association among photospheric cancellations, filament formations, and EUV brightenings with more high resolution and will have basic informations about filament formations.

Acknowledgment

I express my appreciation my supervisor professor Yokoyama Takaaki. This study can not be done without his helpful advices and fruitful discussions. I am very happy to spend my years in his laboratory.

I would like to thank Ichimoto K., Shibata K., Tsuneta S., and Hoshino M. for helpful comments. I also thank for all members of *Hinode* team, graduate school of science of Kyoto Univ. and Nobeyama Solar Radio Observatory. This study can not be done without *Hinode*, SMART/Hida Observatory, and SOHO. We greatly thank for the observers of these instruments very much. We also use the computers of Nobeyama. I would like to thank the students of Solar terrestrial physics group of Univ. of Tokyo, Kyoto Univ. and NAOJ. They gave many advices and comments on this study.

Hinode is a Japanese mission developed and launched by ISAS/JAXA, collaborating with NAOJ as a domestic partner, NASA and STFC (UK) as international partners. Scientific operation of the Hinode mission is conducted by the Hinode science team organized at ISAS/JAXA. This team mainly consists of scientists from institutes in the partner countries. Support for the post-launch operation is provided by JAXA and NAOJ (Japan), STFC (U.K.), NASA, ESA, and NSC (Norway). This work was partly carried out at the NAOJ Hinode Science Center, which is supported by the Grant-in-Aid for Creative Scientific Research ”The Basic Study of Space Weather Prediction” from MEXT, Japan (Head Investigator: K. Shibata), generous donations from Sun Microsystems, and NAOJ internal funding.

I thank to my parents. I could not have continued this thesis without their financial and mental supports.

Bibliography

[1] Aschwanden, M. J., 2004, Physics of the Solar Corona. An Introduction, p.272

[2] Babcock, H. W. & Babcock, H. D., 1955, The Sun's magnetic field, 1952-1954., *ApJ*, **121**, 349

[3] Chae, J., Moon, Y. J., & Pevtsov, A., 2004, Observational evidence of magnetic flux submergence in flux cancellation sites, *ApJ*, **602**, L65

[4] Harvey, K. L., Jones, H. P., Schrijver, C. J., & Penn, M. J., 1999, Does magnetic flux submerge at flux cancelation sites?, *Sol.Phys.*, **190**, 35

[5] Hirayama, T., 1985, Modern observations of solar prominences, *Sol.Phys.*, **100**, 495

[6] Howard, R., 1959, Observations of solar magnitic Fields., *ApJ*, **130**, 193

[7] Ichimoto, K., Lites, B., Elmore, D., Suematsu, Y., Tsuneta, S., Katsukawa, Y., Shimizu, T., Shine, R., Tarbell, T., Title, A., Kiyohara, J., Shinoda, K., Card, G., Lecinski, A., Streander, K., Nakagiri, M., Miyashita, M., Noguchi, M., Hoffmann, C., & Cruz, T., 2008, Polarization Calibration of the Solar Optical Telescope onboard Hinode, *Sol.Phys.*, **249**, 233

[8] Kosugi, T., Matsuzaki, K., Sakao, T., Shimizu, T., Sone, Y., Tachikawa, S., Hashimoto, T., Minesugi, K., Ohnishi, A., Yamada, T., Tsuneta, S., Hara, H., Ichimoto, K., Suematsu, Y., Shimojo, M., Watanabe, T., Shimada, S., Davis, J. M., Hill, L. D., Owens, J. K., Title, A. M., Culhane, J. L., Harra, L. K., Doschek, G. A., & Golub, L., 2007, The Hinode (Solar-B) Mission: An Overview, *Sol.Phys.*, **243**, 3

[9] Kippenhahn, R., & Schlüter, A., 1957, Eine theorie der solaren filamente. Mit 7 textabbildungen, *Z.f urAstrophys.*, **43**, 36

[10] Kubo, M., & Shimizu, T., 2007, Magnetic field properties of flux cancellation sites, *ApJ*, **671**, 990

[11] Kuperus, M., & Raadu, M. A., 1974, The support of prominences formed in neutral sheets, *A & A*, **31**, 189

[12] Leroy, J. L., 1989, in E. R. Priest (ed.), Dynamics and Structures of Quiescent Solar Prominences, p. 77

[13] Lites, B. W., 2005, Magnetic flux ropes in the solar photosphere: The vector magnetic field under active region filaments, *ApJ*, **622**, 1275

[14] Litvinenko Y. E., & Wheatland M. S., 2005, A simple dynamical model for filament formation in the solar corona, *ApJ*, **630**, 587

[15] Livi, S. H. B., Wang, J., & Martin, S. F., 1985, The cancellation of magnetic flux. I - On the quiet sun, *AustralianJ.phys.*, **38**, 855

[16] A. Lòpez Ariste, G. Aulanier, B. Schmieder, & A. Sainz Dalda, 2006, First observation of bald patches in a filament channel and at a barb endpoint, *A&A*, **456**, 725L

[17] Martens, P. C., & Zwaan, C. 2001, Origin and evolution of filament-prominence systems, *ApJ*, **558**, 872

[18] Martin, S. F., Livi, S. H. B., & Wang, J., 1985, The cancellation of magnetic flux. II - In a decaying active region, *AustralianJ.phys.*, **38**, 929

[19] Martin, S. F. 1990, IAU Colloq. 117, ed. E. Tandberg-Hanssen, Lect. Notes Phys. 363 (Springer-Verlag), 1

[20] Martin, S. F., Bilimoria, R., & Tracadas, P. W., 1994, in R. J. Rutten and C. J. Schrijver (eds.), Solar Surface Magnetism, Kluwer Academic Publishers, Dordrecht, Holland, p. 303.

[21] Martin, S. F., 1998, Conditions for the formation and maintenance of filaments, *Sol.phys.*, **182**, 107

[22] Okamoto, J. T., Tsuneta, S., Berger, T. E., Ichimoto, K., Katsukawa, Y., Lites, B. W., Nagata, S., Shibata, K., Shimizu, T., Shine, R. A., Suematsu, Y., Tarbell, T. D., & Title, A. M., 2007, Coronal transverse magnetohydrodynamic waves in a solar prominence, *Science*, **318**, 1577

[23] Okamoto, J. T., Tsuneta S., Lites, Bruce W., Kubo, M., Yokoyama, T., Berger, Thomas E., Ichimoto, K., Katsukawa, Y., Nagata, S., Shibata, K., Shimizu, T., Shine, R. A., Suematsu, Y., Tarbell, T. D., & Title, A. M., 2008, Emergence of a Helical Flux Rope under an Active Region Prominence, *ApJ*, **672**, L215

[24] Rust, D. M., & Kumar, A. 1994, Helical magnetic fields in filaments, *Sol.Phys.*, **155**, 69

[25] Schmieder, B., Aulanier, G., & Mein, P., 2006, Evolving photospheric flux concentrations and filament dynamic changes, *Sol.Phys.*, **238**, 245

[26] Scherrer, P. H., Bogart, R. S., Bush, R. I., Hoeksema, J. T., Kosovichev, A. G., & Schou, J., 1995, The solar oscillations investigation - Michelson Doppler Imager, *Sol.Phys.*, **162**, 129

[27] Shimizu, T., Nagata, S., Tsuneta, S., Tarbell, T., Edwards, C., Shine, R., Hoffmann, C., Thomas, E., Sour, S., Rehse, R., Ito, O., Kashiwagi, Y., Tabata, M., Kodeki, K., Nagase, M., Matsuzaki, K., Kobayashi, K., Ichimoto, K., & Suematsu, Y., 2008, Image stabilization system for Hinode (Solar-B) Solar optical Telescope, Solar Physics, *Sol.Phys.*, **249**, 221

[28] Suematsu, Y., Tsuneta, S., Ichimoto, K., Shimizu, T., Otsubo, M., Katsukawa, Y., Nakagiri, M., Noguchi, M., Tamura, T., Kato, Y., Hara, H., Mikami, I., Saito, H., Matsushita, T., Kawaguchi, N., Nakaoji, T., Nagae, K., Shimada, S., Takeyama, N., & Yamamuro, T., 2008, The Solar Optical Telescope of Solar-B: the Optical Telescope Assembly, *Sol.Phys.*, **249**, 197

[29] Tandberg-Hanssen, E., 1995, The nature of solar prominences

[30] Tsuneta, S., Ichimoto, K., Katsukawa, Y., Nagata, S., Otsubo, M., Shimizu, T., Suematsu, Y., Nakagiri, M., Noguchi, M., Tarbell, T., Title, A., Shine, R., Rosenberg, W., Hoffmann, C., Jurcevich, B., Kushner, G., Levay, M., Lites, B., Elmore, D., Matsushita, T., Kawaguchi, N., Saito, H., Mikami, I., Hill, L. D., & Owens, J. K., 2008, The Solar Optical Telescope for the Hinode Mission: An Overview, *Sol.Phys.*, **249**, 167

[31] UeNo, S., Nagata, S., Kitai, R., & Kurokawa, H., 2004, Features of solar telescopes at the Hida Observatory and the possibilities of coordinated observations with SolarB, ASP Conf., **325**, 319

[32] van Ballegooijen, A. A., & Martens, P. C. H., 1989, Formation and eruption of solar prominences, *ApJ*, **343**, 971

[33] Welsch, B. T., DeVore, C. R., & Antiochos, C. K., 2005, Magnetic reconnection models of prominence formation, *ApJ*, **634**, 1395

[34] Wood, P., & Martens, P. C., 2003, Measurements of flux cancellation during filament formation, *Sol.Phys.*, **218**, 123

[35] Zwaan, C., 1987, Elements and patterns in the solar magnetic field, *ARA&A*, **25**, 83